Life-cycle analysis of last-mile parcel delivery using autonomous delivery robots

Clément Lemardelé [a,c,*], Sofia Pinheiro Melo [b], Felipe Cerdas [b], Christoph Herrmann [b], Miquel Estrada [c]

[a] *CARNET – Future Mobility Research Hub. C. Jordi Girona 29, Building Nexus II, Office 0A, 08034 Barcelona, Spain*
[b] *Chair of Sustainable Manufacturing & Life Cycle Engineering, Institute of Machine Tools and Production Technology (IWF), Technische Universität Braunschweig, Langer Kamp 19b, 38106 Braunschweig, Germany*
[c] *Civil Engineering School of Barcelona, Department of Civil and Environmental Engineering, Universitat Politècnica de Catalunya – Barcelona TECH, C. Jordi Girona 1-3, Building B1, North Campus, 08034 Barcelona, Spain*

ARTICLE INFO

ABSTRACT

The acceleration of global e-commerce brings an increasing environmental burden to urban last-mile logistics. Autonomous delivery robots (ADRs) have often been considered as an attractive solution to this challenge but, to date, their environmental impact had not been fully assessed. To fill this gap, a life-cycle analysis of two-echelon and business-as-usual distribution strategies is proposed in this paper. To model ADR production, primary data from an actual prototype is used. The mathematical formulation of the use stage is done using the continuous approximation methodology. Finally, some managerial insights are obtained. Two-echelon operations would generate between 60 and 130 gCO$_2$-eq per parcel delivery depending on the considered operation scenario. The ADR fleet production and renewal are the biggest contributors to this total global warming potential (GWP). As a consequence, the three main leverages to decrease the GWP of an ADR-based two-echelon delivery scheme are an improvement of the ADR production processes, the maximization of the robot lifespan (both for mechanical parts and battery), and the optimization of delivery operations to minimize the robot fleet size.

1. Introduction and state of the art

The use of autonomous delivery robots (ADRs) for last-mile delivery has been attracting growing market interest over the last years, particularly driven by the ongoing COVID-19 pandemic and its need for contactless package deliveries (Pani et al., 2020). However, given the growing demand for last-mile deliveries and their associated environmental impacts, understanding to what extent new technologies, such as automation and robotics, can help reducing the environmental impacts of last-mile deliveries is becoming increasingly relevant. By exploring the different delivery strategies (i.e. using human-driven or autonomous vehicles with human delivery, ground robots or drones) and powertrains, research has been focusing on new business models to find applications and solutions to improve last-mile logistics, the most carbon intensive and least energy efficient supply chain link (Li et al., 2021).

Using a life cycle assessment (LCA) framework, Li et al. (2021) investigated the key parameters influencing the life cycle greenhouse gas (GHG) emissions of package delivery scenarios, benchmarking the use of electric and gas-powered autonomous vehicles and

---

* Corresponding author at: CARNET – Future Mobility Research Hub. C. Jordi Girona 29, Building Nexus II, Office 0A, 08034 Barcelona, Spain.
  E-mail address: clement.lemardele@upc.edu (C. Lemardelé).

two-legged robot against the traditional delivery method with driver hand-delivering parcels. It was found that full automation does not reduce the emissions in comparison with conventional delivery, which is associated with the lowest emissions with the use of electric vehicles (EVs). Given the superior relevance of the electrification of the powertrain in comparison with vehicle automation, the need for decarbonizing the grid is also highlighted.

Aiming to investigate the life cycle environmental impact of the electrification of the powertrain in the delivery of goods in urban environments, Marmiroli et al. (2020) compared three light commercial vehicles (LCVs) with diesel, compressed natural gas and electric powertrains, using primary data from the vehicles' manufacturer, considering a standard delivery mission. While in the production stage, the impacts are higher for the electric version in all the analyzed impact categories, during the usage its environmental performance could be superior to internal combustion engine vehicle (ICEV) versions in some categories, assuming a renewable-based electricity mix use scenario.

In the context of autonomous vehicles, connected and automated vehicles (CAVs) can combine connectivity (i.e. ability to share information with a connected vehicle and an infrastructure network) and automation technologies, being classified into five levels, from zero to full automation. Kemp et al. (2020) investigated life cycle energy usage and GHG emissions of Level 4 CAVs (i.e. high automation) by conducting an LCA of CAV platforms for electric sport utility vehicles (SUVs) and ICE vans, as part of an automated taxi fleet. By analyzing different scenarios varying the grid carbon intensity, and computing power requirements, 31% potential reduction of life cycle GHG emissions is expected when considering low carbon grid (0.08 kg CO_2-eq/kWh) for CAV battery electric vehicles (BEVs), compared to the base scenario, whereas an increase of 34% is computed for high power (4000 W). This study reveals the importance of reducing CAV subsystem power requirements, as well as the vehicle electrification, together with grid decarbonization, towards a more sustainable implementation of CAV technology.

Drones are also being explored as a way towards more environmentally sustainable technologies in the delivery systems. Focusing on the usage stage, Figliozzi (2020) revealed the potential of air (drones) and ground (sidewalk and road types) ADRs to reduce the carbon emissions, and analyzed the key influencing factors when comparing store delivery with in-store shopping. While studies have shown the environmental benefits of drone's delivery (Koiwanit, 2018; Park et al., 2018; Stolaroff et al., 2018), drones are associated with major shortcomings (e.g. air safety and congestion, given the risk of system malfunction or hacking, and intense air traffic to meet
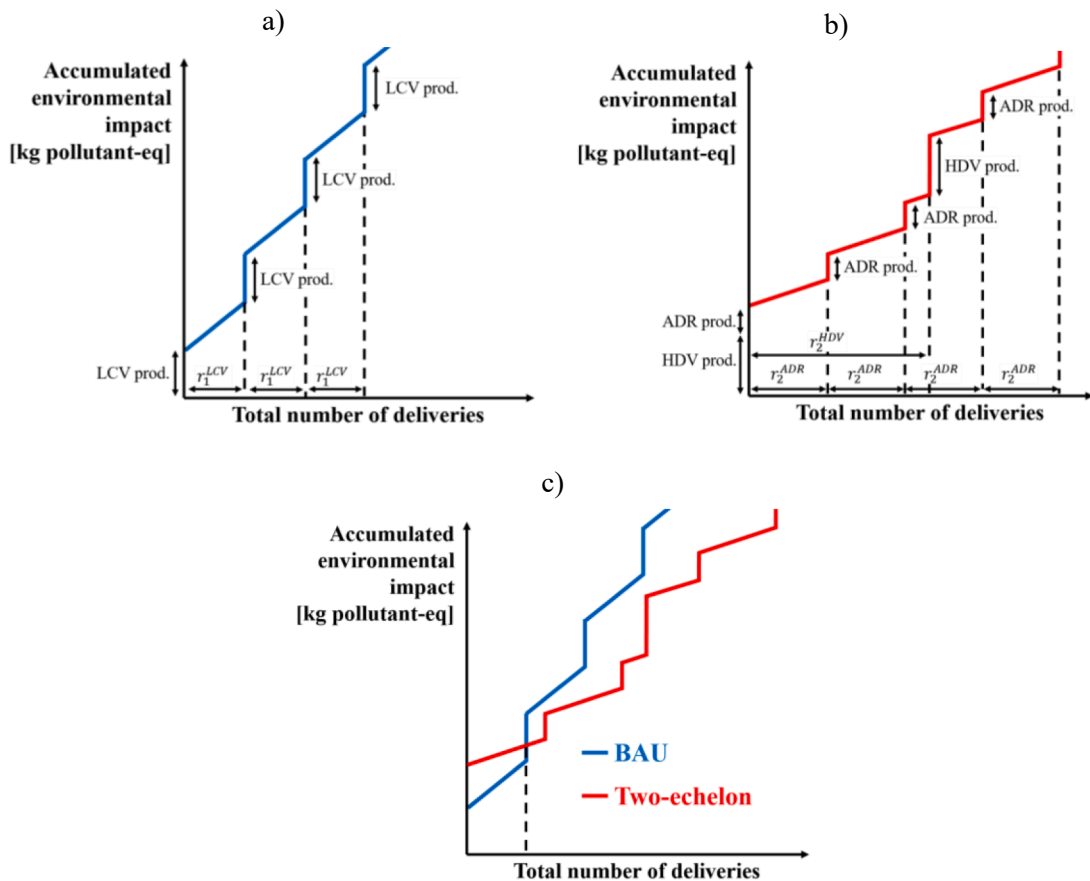

Fig. 1. Expected accumulated environmental impact of (a) BAU and (b) two-echelon delivery scenarios. BAU and two-echelon delivery scenarios accumulated environmental impacts are compared in (c).

the delivery demand) and are more efficient in time-constrained and low-density delivery contexts (Figliozzi, 2020).

Comparing them with ICEVs and EVs for grocery delivery, Yowtak et al. (2020) revealed that unmanned air vehicles (UAVs) are currently not competitive in terms of environmental and economic aspects. Even though UAVs supplemented with ICEV delivery on poor weather days (i.e. they are mostly unable to operate in rain or snow conditions) have the potential to perform better than the ICEV-only operation with regards to GHG emissions, environmental impacts such as photochemical oxidant formation potential and respiratory effects are increased. In addition, the energy required per km for high-payload UAVs is significantly greater than for EV systems, hence leading to higher environmental impacts when considering UAVs supplemented with EVs, in comparison with EVs-only scenario (Yowtak et al., 2020).

While previous studies have analyzed the technical and environmental feasibility of autonomous vehicles, two-legged robots, drones, as well as the electrification of the powertrain for delivery systems, very little is known about the potential of ADRs to reduce the environmental impact of last-mile deliveries. The impact from the production of the ADRs and their use in an urban context is still subject of investigation. In this way, this paper focuses on providing a holistic approach of last-mile logistics operations, adopting a cradle-to-grave perspective; from the extraction of raw materials, through the production, up to the use stage. In order to model the production burdens, primary data from an ADR prototype manufacturer will be used. The delivery scenario mathematical formulation is based on the continuous approximation (CA) methodology (Daganzo et al., 2012). To the best of our knowledge, such a holistic approach, that combines primary ADR data and accurate usage stage formulation, has not been done yet.

Two delivery strategies will be investigated and compared: business-as-usual (BAU) and two-echelon. In the BAU scheme, LCVs directly take the parcels from the carrier's distribution center (DC) to the final receivers that are located in the considered service area. In the two-echelon scheme, the parcels are firstly taken from the carrier's DC to some micro-hubs using heavy-duty vehicles (HDVs), being then transshipped from the HDVs to the ADRs at the micro-hubs. Secondly, ADRs deliver the parcels from the micro-hubs to the final customers. A detailed description of these delivery strategies can be found in the next chapter.

In this context, one of our main objectives in this study is to explore the improvements in the operational efficiency generated by the implementation of a two-echelon delivery pattern (Soysal et al., 2015). The question is whether these improvements will result in
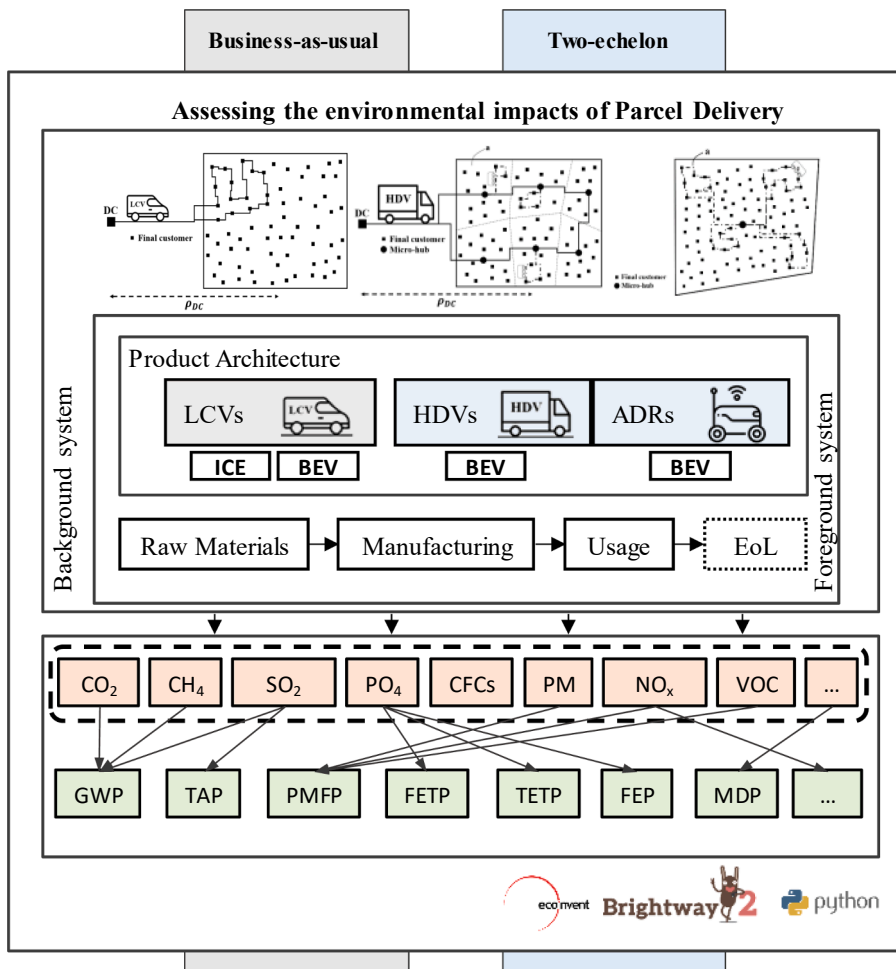

Fig. 2. Modelling framework based on LCA for assessing the environmental impacts of parcel delivery systems.

lower energy consumption during the usage stage, and eventually decrease the environmental impact of last-mile delivery operations. To address this question, fleet replacements will be also considered. In the BAU scheme, a number of LCVs are first produced and then replaced every r_1^{LCV} deliveries (see Fig. 1a). In the two-echelon delivery scheme, two fleets have to be considered. On the one hand, HDVs are first produced and replaced every r_2^{HDV} deliveries. On the other hand, a number of ADRs are also produced and replaced every r_2^{ADR} deliveries (see Fig. 1b). In Fig. 1, the slope of each segment actually corresponds to the environmental impact associated with the energy consumption per parcel delivery in both the BAU and two-echelon use stages, while the discontinuities represent the expected environmental impact of fleet replacements.

As illustrated in Fig. 1c, the primary aim is to compare the accumulated environmental impacts from BAU and two-echelon schemes over the lifetime. While it might be expected that the total vehicle production impact is higher in the two-echelon scheme, since many ADRs would be needed to make all the deliveries (i.e. they operate at a lower speed than LCVs and have a lower volume capacity), in the end, the energy savings during the usage stage might lead to a more environmentally sustainable two-echelon model (see Fig. 1c). This tradeoff between production and usage stage has been addressed in the LCA literature (Hauschild et al., 2018), in the context of integrated life cycle engineering (IC-LCE) framework (Cerdas et al., 2022) and already studied for other vehicles (e.g. for the case of electric vehicles, see Marmiroli et al., 2020, and for electric aircrafts, see Melo et al., 2022). However, an analysis of this potential tradeoff for the case of ADRs operating in two-echelon delivery schemes is still missing. Motivated to address this research gap, we aim at extending these findings to the field of last-mile logistics.

2. Methodology

This chapter describes the LCA-based framework and modelling approach developed in this study to address the aforementioned research question. Each section of the framework is addressed, particularly the LCA methodological aspects for modelling the environmental impacts. This is followed by a detailed description of the system modelling; distinguishing between BAU and two-echelon schemes, considering the production and usage of the vehicles operated in each of the investigated delivery schemes. In the end, the uncertainty present in the modelling stage is addressed.

2.1. Framework

Fig. 2 presents the developed LCA-based modelling framework. The focus of investigation lies on the modelling and comparison between the BAU (i.e. using ICE- or BEV-LCVs) and two-echelon delivery schemes (i.e. using ADRs and BEV-HDVs) in terms of energy consumption and environmental impacts, assuming the vehicles being operated in a particular city. For this purpose, the framework highlights the foreground system of both delivery schemes, considering their vehicle and powertrain architectures and the systems in the background relevant for vehicle's operation. Setting the context of the LCA, the methodological phases such as defining the goal and scope, the inventory analysis, impact assessment and interpretation are addressed.

LCA is a methodology for systematically analyzing and evaluating the environmental impacts of a product system over its entire life cycle (i.e from raw material extraction, manufacturing, usage to final disposal or recycling), following the ISO 14040/14044 standards (Hauschild et al., 2018). LCA studies can be used to identify problem shifting, such as the shifting of the environmental burdens between impact categories or life cycle stages when comparing alternatives, enabling an understanding of the real implications associated with a product system throughout its life cycle.

As illustrated in Fig. 2, a distinction is typically made in terms of foreground system (the system being directly engineered, e.g. the vehicle, the robot) and the background system (the systems that we need to operate our vehicle, e.g. the energy system, the material supply chain). While performing an LCA, data on all input flows (e.g. materials, resources and energy) and output flows (e.g. waste, emissions and products) related to the product system under analysis are collected and compiled in a so-called life cycle inventory (LCI). The inventory flows can then be characterized into corresponding environmental impacts based on an impact assessment method (as shown in Fig. 2). For the production of the ADRs, the impact assessment is based on the fourteen impact categories listed in

Table 1
ReCiPe impact categories investigated in this study.

Abbreviation	Impact Category	Unit
GWP100	Global Warming Potential	kg CO_2-eq.
ODPinf	Ozone Depletion Potential	kg CFC-11-eq.
FEP	Freshwater Eutrophication Potential	kg P-eq.
MEP	Marine Eutrophication Potential	kg N-eq.
IRP_HE	Ionizing Radiation	kg U235-eq.
FETPinf	Freshwater Toxicity Potential	kg 1.4-DCB-eq.
PMFP	Particulate Matter Formation	kg PM10-eq.
POFP	Photochemical Oxidant Formation	kg NMVOC
METPinf	Marine Toxicity Potential	kg 1.4-DCB-eq.
TETPinf	Terrestrial ecotoxicity	kg 1.4 DCB-eq.
HTPinf	Human Toxicity Potential	kg 1.4-DCB-eq.
TAP100	Terrestrial Acidification	kg SO_2-eq.
MDP	Metal Depletion	kg Fe-eq.
FDP	Fossil Depletion	kg oil-eq.

Table 1 according to the ReCiPe method, commonly used for environmental assessment (Goedkoop et al., 2013). While the selected impact categories allow a broader analysis of the emissions, the focus in this paper will mainly lie on the global warming potential (GWP), since it is commonly investigated in the field of LCA for last-mile logistics (Li et al., 2021; Kemp et al., 2020; Stolaroff et al., 2018). The impact assessment is then followed by the interpretation of results, analyzing the environmental impacts resulting from the LCI. To provide the needed background information on materials and energy carriers, the Ecoinvent 3.6 database is used. For all LCA calculations, Brightway2 framework is used, applying python programming language in jupyter notebooks.

As addressed in the Introduction, this paper's main goal is to quantify the environmental impact of the BAU and two-echelon delivery schemes (to be defined in the following subsection 2.1.1) and compare them. A comparative analysis is needed to understand to what extent the efficiency improvements with the use of ADRs will contribute to reduce the environmental impact of last-mile delivery operations. The supply chain under study is mainly the e-commerce delivery market in which the demand is more fragmented. Due to the lack of data, the end-of-life (EoL) modelling is beyond the scope of investigation. It is taken into account the extraction of raw materials, manufacturing up to the usage stage of vehicles operating in both delivery schemes. The functional unit (FU) is the delivery of 1 parcel to 1 receiver, assuming that 1 customer receives one parcel. Temperature-controlled parcels are not considered. Two particular case studies will be analyzed: Hamburg (HH) and Barcelona (BCN) urban cores (Dijkstra et al., 2019). However, the operation models (to be introduced the next in Section 2.2) developed for these studies can be applied to any other given city or service region.

2.2. System modelling

The BAU and two-echelon are the delivery schemes considered for investigation. To ensure a fair comparison, the same FU, i.e. the delivery of one parcel to one final recipient, and constraints (time window, service region, demand density, etc.) will be considered.

2.2.1. Business-as-usual delivery scheme

In this delivery scheme, LCVs (see Fig. 3) directly take the parcels from the carrier's distribution center (DC) to the final receivers that are located in the considered service area. The objective of the carrier is to minimize the distance travelled by its fleet in the given time window H considering that the volume capacity of the LCVs is limited. This is a particular instance of the capacitated vehicle routing problem with time window (CVRPTW, see Baldacci et al., 2012).

Either diesel ICE or battery-electric LCVs (BEV-LCVs) will be considered. In the case of BEV-LCVs, we assume that they are recharged at the DC (they cannot be recharged along their delivery route). The distance from DC to the center of the service region is given by ρ_{DC}.

(a) Environmental impact from the production of LCVs.

Data from Ellingsen et al. (2016), originated from the inventories developed by Hawkins et al. (2012), has been used to calculate the GWP from the production of the LCVs. In the case of BEV-LCVs, the vehicle without batteries was considered, computing the battery production burdens separately. Data from the "BenchBatt" project (see Cerdas et al., 2018), was used considering a lithium iron phosphate (LFP) battery, which is the technology currently used in the ADR prototype. The GWP data and the battery specifications are summarized in Melo et al. (2020).

(b) Environmental impact from the use of LCVs.

Concerning the LCV use stage, the estimation of the GWP_u of a vehicle veh, travelling on a road s, for a distance d_s^{veh} is given in Equation (1).

$$GWP_u\left(veh, s, d_r^{veh}\right) = gwp^{fuel} z_s^{veh} d_s^{veh} \tag{1}$$

Where gwp^{fuel} [kg CO_2-eq/kWh] is the well-to-wheel GWP of 1 kWh of energy carrier (either diesel or electricity), and z_s^{veh} [kWh/km] the expected unit distance energy consumption of vehicle veh on road s.

The estimation of gwp^{fuel} is described in Chapter 3. The unit distance expected energy consumption z_s^{veh} is computed using the technical characteristics of the vehicle and considering several driving cycles (see Supplementary Information, section 2).

Finally, the distances travelled by the vehicle fleets in the considered use cases are estimated using the continuous approximation methodology (Daganzo, 2012). The modelling is detailed in the following section.

(c) Modelling the operation of LCVs.

In this scenario, the LCVs directly go from the DC to the final receivers' locations (as illustrated in Fig. 3). The first step of the modelling process is to estimate the expected distance between two consecutive receivers l_1^{LCV} [km] (Daganzo, 1984).
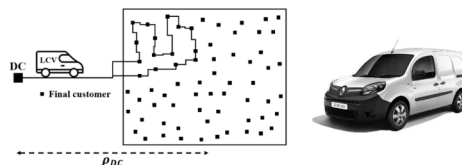

Fig. 3. BAU delivery scheme with LCVs (Renault, 2021).

$$l_1^{LCV} = \frac{k^{LCV}}{\sqrt{\delta}} \tag{2}$$

Where the LCV expected routing factor k^{LCV} is a coefficient that depends on the service region road grid and δ [receivers/km^2/day] the total demand density per logistics operator.

Then the LCV expected delivery time t_1^{LCV} [h], including access and stop times, is estimated in Equation (3).

$$t_1^{LCV} = \frac{l_1^{LCV}}{\overline{v}_L^{LCV}} + \tau_d^{LCV} \tag{3}$$

Where $\overline{v}_L^{LCV}$ [km/h] is the LCV expected commercial speed in the local urban grid (calculation can be found in the Supplementary Information, section 2), and τ_d^{LCV} [h] the LCV expected stop time per delivery.

To estimate the energy consumption in this BAU Scenario 1, it is necessary to have an estimation of the number of routes needed to visit all the receivers, given the constraints of the problem.

The first step is to estimate the expected number of receivers visited along one LCV route Ψ_1^{LCV}. The value of Ψ_1^{LCV} is constrained by three main restrictions: the LCV limited volume capacity, the operation time horizon H allowed and the LCV limited battery capacity. Ψ_1^{LCV} is also equal to the number of parcels loaded in the LCV at the beginning of its route, assuming that one receiver gets one parcel.

In Equation (4), Ψ_1^v represents the maximum number of receivers that could be visited per LCV route if only the LCV volume capacity constraint were considered.

$$\Psi_1^v = \frac{C^{LCV}}{E(u)} \tag{4}$$

Where C^{LCV} [m^3] is the LCV volume capacity and $E(u)$ [m^3] the parcel expected volume.

If only the time horizon constraint were considered, Ψ_1^t receivers could be visited along each individual LCV route.

$$\Psi_1^t = \frac{H - \frac{2\rho_{DC}}{\overline{v}_{LH}^{LCV}}}{t_1^{LCV}} \tag{5}$$

Where $\overline{v}_{LH}^{LCV}$ [km/h] is the LCV expected commercial speed on metropolitan highways (calculation can be found in the Supplementary Information, section 2), and ρ_{DC} the expected distance between the DC and the service region (see Fig. 3).

Finally, if only the LCV limited battery capacity restriction were considered, Ψ_1^b receivers could be visited along each LCV route. Ψ_1^b is the solution of Equation (6).

$$\Psi_1^b l_1^{LCV} z_L^{LCV}\left(\Psi_1^b\right) + 2\rho_{DC} z_{LH}^{LCV}\left(\Psi_1^b\right) = BC^{LCV} \tag{6}$$

Where z_L^{LCV} [kWh/km] is the LCV expected unit distance energy consumption in the local urban grid, z_{LH}^{LCV} [kWh/km] the LCV expected unit distance energy consumption on metropolitan highways and BC^{LCV} [kWh] the LCV battery effective energy capacity (assuming a rate of discharge of 80%). Please refer to the Supplementary Information (section 2) for the calculation of z_L^{LCV} and z_{LH}^{LCV}.

In the case of diesel ICE LCVs, we do not consider this constraint of limited battery capacity.

Finally, Ψ_1^{LCV} is equal to the minimum value between Ψ_1^v, Ψ_1^t and Ψ_1^b, ensuring that the three restrictions are enforced.

$$\Psi_1^{LCV} = min\left\{\Psi_1^v; \Psi_1^t; \Psi_1^b\right\} \tag{7}$$

In the case of diesel ICE LCVs, Ψ_1^{LCV} is equal to the minimum value between Ψ_1^v and Ψ_1^t only.

The total distance travelled by the LCV fleet on metropolitan highways D_1^{LH} [veh-km] is computed in Equation (8).

$$D_1^{LH} = 2\rho_{DC}\left[\frac{\delta A}{\Psi_1^{LCV}}\right]^+ \tag{8}$$

Where $[x]^+$ represents the upper integer of x.

D_1^L [veh-km/day] is the total distance travelled by the LCV fleet in the local urban grid.

$$D_1^L = k^{LCV} A \sqrt{\delta} \tag{9}$$

T_1 [veh-h/day] is the total time worked by the LCV fleet.

$$T_1 = \frac{D_1^{LH}}{\overline{v}_{LH}^{LCV}} + \frac{D_1^L}{\overline{v}_L^{LCV}} + \delta A \tau_d^{LCV} \tag{10}$$

E_1^{LCV} [kWh/day] is the LCV fleet total energy consumption in this BAU Scenario.

$$E_1^{LCV} = D_1^{LH} z_{LH}^{LCV}\left(\Psi_1^{LCV}\right) + D_1^L z_L^{LCV}\left(\Psi_1^{LCV}\right) \tag{11}$$

The expected LCV fleet size in BAU Scenario 1 N_1^{LCV} is estimated in Equation (12) (calculation can be found in the Supplementary Information, section 3, result 1).

$$\begin{cases} If \dfrac{E_1^{LCV}}{BC^{LCV}} \geq \dfrac{T_1}{H}; N_1^{LCV} = \left[\dfrac{T_1 + \dfrac{E_1^{LCV}}{P_c^{LCV}}}{H + \dfrac{BC^{LCV}}{P_c^{LCV}}}\right]^+ \\ \\ If \dfrac{E_1^{LCV}}{BC^{LCV}} \leq \dfrac{T_1}{H}; N_1^{LCV} = \left[\dfrac{T_1}{H}\right]^+ \end{cases} \qquad (12)$$

Where P_c^{LCV} [kW] is the LCV battery charging power.

In the case of diesel ICE LCVs, the expected fleet size is equal to the ratio $[T_1/H]^+$ because there is no constraint concerning the vehicle's limited battery capacity.

The expected number of parcels delivered between two LCV fleet replacements r_1^{LCV} (see Fig. 1) is given in Equation (13) (see the Supplementary Information, section 3, result 2).

$$r_1^{LCV} = \delta A \bullet min\left\{\dfrac{CL^{LCV}BC^{LCV}N_1^{LCV}}{E_1^{LCV}}; \dfrac{L^{LCV}N_1^{LCV}}{D_1^{LH} + D_1^L}\right\} \qquad (13)$$

Where CL^{LCV} [number of cycles] is the LCV battery expected cycle life, and L^{LCV} [km] the LCV maximum lifespan.

We assume that an LCV has to be substituted by a new one if its battery reaches its maximum number of cycles or the vehicle (especially the mechanical parts) reaches its maximum lifespan.

In the case of diesel ICE LCVs, r_1^{LCV} is equal to $\delta A \dfrac{L^{LCV}N_1^{LCV}}{D_1^{LH} + D_1^L}$.

2.2.2. Two-echelon delivery scheme

In this alternative scenario, the considered service region is divided into N_h delivery zones (DZs) of expected area a (see Fig. 4). Within each DZ, a logistics facility (micro-hub) is created.

In the first echelon of the distribution process, the parcels are taken from the carrier's DC to the micro-hubs using heavy-duty vehicles (HDVs) to take advantage from their bigger volume capacity and increase the economies of scale (see Fig. 4a). The parcels are then transshipped from the HDVs to ADRs at the micro-hubs. Once all the parcels corresponding to a given delivery zone have been unloaded, the HDV goes to the next micro-hub. This process is repeated until all the micro-hubs are visited by the HDV fleet.

In the second echelon, ADRs deliver the parcels from the micro-hubs to the final customers (see Fig. 4b). The operations of ADRs are characterized by a higher number of routes from the micro-hub to the receivers (because they have a smaller volume capacity), travelled at a lower speed. This optimization problem is a particular instance of the two-echelon capacitated vehicle routing problem with a time window constraint (Soysal et al., 2015).

It is assumed that both HDVs and ADRs are BEVs that can be recharged at the carrier's DC (for the HDVs) and at the micro-hubs (for the ADRs). The objective of implementing urban logistics micro-hubs directly within the service region is to minimize the distance
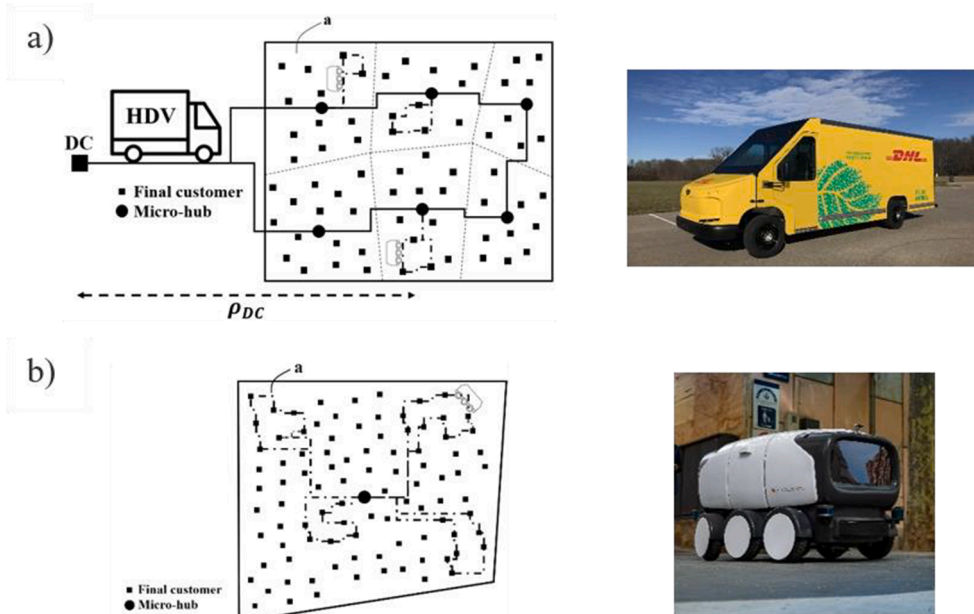

Fig. 4. Two-echelon delivery operations with HDVs (StreetScooter, 2021) and ADRs.

travelled by the ADRs to access the final receivers, because these vehicles have a lower battery capacity, i.e. a lower range than HDVs. Designing representative energy consumption models and efficient energy management systems, especially under different payload scenarios, is a crucial challenge to ensure an optimal deployment of battery-electric micro-vehicles, such as ground ADRs or air delivery drones (Alyassi et al., 2022; Bruni et al., 2023; Liu, 2023; Torabbeigi et al., 2020).

a) Environmental impact from the production of HDVs and ADRs.

2.2.3. HDV production

Similar to the case of LCVs, data from Ellingsen et al. (2016), originated from the inventories developed€ by Hawkins et al. (2012), has been used to calculate the GWP from the production of the HDVs. The battery production burdens have also been computed separately, using data from the "BenchBatt" project, see Cerdas et al. (2018), summarized in Melo et al. (2020). A lithium iron phosphate (LFP) battery is considered in the case of electric HDVs.

2.2.4. ADR production modelling

The production of the ADR is modeled using primary data from the ADR's prototype manufacturer, being divided into twelve main sub-components, i.e. *chassis, external shell, brakes, steering axis, batteries, motors, wheels and tires, internal delivery system, electronics, sensors, processing units and communication interfaces and display equipment.* Table 2 shows the material decomposition of the ADR prototype, whereas Table S1 in the Supplementary Information shows the developed LCI of each component, which was determined from the designed prototype. The data from the background system on raw materials and energy is modeled via the Ecoinvent 3.6 database. The LCI also computes the transportation of raw materials, and components, from raw material extraction up to production. The transport distances between the locations are covered by trucks, container ships, or trains. It is assumed that the production of the sub-components takes place in China, being transported to Portugal, where the ADR is assembled.

The fabrication processes of the sub-components made of steel and aluminum are modeled using Ecoinvent 3.6 datasets (see Table S1 in the Supplementary Information). Plastics present in the prototype include POM, PET, PP, PVC, epoxy resin, flexible foam, polycarbonate, synthetic rubber, glass fiber reinforced plastics (CFRP) and 3D-printed elements (PLA). For 3D-printed elements, data from Cerdas et al. (2017) is considered. For CFRP, the hand lay-up technique is assumed given its reduced cost (Cucinotta et al., 2017).

The electric motors present in the ADR are modeled using the Ecoinvent 3.6 dataset for electric scooter (Hollingsworth et al., 2019). The life-cycle inventory of the sensors present in the robot, i.e. LiDARs, sonars and cameras, follows the methodology proposed by Gawron et al. (2018). Concerning the brake system, due to lack of data, it was assumed to be composed of 90% of aluminum and 10% of synthetic rubber. Brakes represent approximately 1% of the total mass of the ADR, making this assumption acceptable. To model the wheels and tires, data from Hawkins et al. (2013) is used considering an energy consumption of 0.11 kWh per kg of synthetic rubber for the vulcanization process (Cobert, 2009). Finally, steppers, potentiometers, li-ion batteries, and liquid crystal display are modeled using Ecoinvent 3.6 datasets. Further details can be found in the Supplementary Information (see Table S1).

(b) Environmental impact from the use of HDVs and ADRs.

Concerning the HDVs and ADRs usage stage, the estimation of the GWP_u of a vehicle *veh*, travelling on a road *s*, for a distance d_s^{veh} is also given the Equation (1), see Section 2.2.1(b). The well-to-wheel GWP of electricity [kg CO_2-eq/kWh] is described in Chapter 3, and the expected unit distance energy consumption is computed using the technical characteristics of the vehicles and considering several driving cycles (please refer to the section 2 in the Supplementary Information). Regarding the estimation of distances travelled by the vehicle fleets in the considered use cases, the continuous approximation methodology is used (Daganzo, 2012). The modelling is detailed in the next section.

c) Modelling the operation of HDVs and ADRs.

In this subsection, we model the operations of both the HDV and ADR fleets. The considered service region is divided into N_h delivery zones (DZs) of expected area *a* (see Fig. 4). Within each DZ, a logistics facility (micro-hub) is created.

$$N_h = \frac{A}{a}$$

(14)

Table 2
ADR prototype material decomposition.

	Low-alloyed steel (kg)	Aluminum (kg)	Plastics (kg)	Other (kg)	Total (kg)
Internal delivery system	12	0.35	4.8	1.4	18.5
Chassis	9.7	71	–	–	81
External shell	–	5.4	40	–	45
Brakes	–	2.9	–	0.32	3.2
Steering	0.85	–	0.26	–	1.1
Wheels and tires	19	–	7.2	5.3	31
Electronics, sensors, processing units	–	–	–	10	10
Display equipment	–	–	–	8.9	8.9
Batteries	–	–	–	27.5	27.5
Electric motors	–	–	–	32.4	32.4
Total					259

2.2.5. HDV operation modelling

To determine the total number of HDV routes needed to serve all the logistics micro-hubs within the time window H, we first need to estimate the total number of parcels loaded in one HDV at the beginning of its route Ψ_2^{HDV} (see the Supplementary Information, section 3, result 3).

$$\Psi_v^{HDV} = \frac{C^{HDV}}{E(u)} \tag{15a}$$

$$\Psi_t^{HDV} = \frac{H - \frac{2\rho_{DC}}{\bar{v}_{LH}^{HDV}}}{\frac{1}{\delta a}\left(\frac{1}{\bar{v}_L^{HDV}}k^{HDV}\sqrt{a} + \tau_{LU}^{HDV}\delta a\right)} \tag{15b}$$

$$2\rho_{DC}z_{LH}^{HDV}\left(\Psi_b^{HDV}\right) + \Psi_b^{HDV}\frac{k^{HDV}}{\delta\sqrt{a}}z_L^{HDV}\left(\Psi_b^{HDV}\right) = BC^{HDV} \tag{15c}$$

$$\Psi_2^{HDV} = min\left\{\Psi_v^{HDV}; \Psi_t^{HDV}; \Psi_b^{HDV}\right\} \tag{15d}$$

Where C^{HDV} [m^3] is the HDV volume capacity, τ_{LU}^{HDV} [h] the expected time needed to unload one parcel from the HDV at the micro-hub, $\bar{v}_{LH}^{HDV}$ [km/h] the HDV expected commercial speed on line-haul metropolitan highways, k^{HDV} the HDV expected routing factor in the local urban grid, $\bar{v}_L^{HDV}$ [km/h] the HDV expected commercial speed in the local urban grid and BC^{HDV} [kWh] is the HDV effective battery capacity. Please refer to the Supplementary Information (section 2) for the calculation of $\bar{v}_{LH}^{HDV}$, $\bar{v}_L^{HDV}$, as well as z_{LH}^{HDV} and z_L^{HDV}.

The distance travelled on line-haul metropolitan highways by the HDV fleet D_2^{LH} [veh-km] is thus given by

$$D_2^{LH} = 2\rho_{DC}\left[\frac{\delta A}{\Psi_2^{HDV}}\right]^+ \tag{16}$$

The distance D_2^L [veh-km] travelled by the HDV fleet in the local urban grid is given by Equation (17).

$$D_2^L = k^{HDV}\sqrt{AN_h} = k^{HDV}\frac{A}{\sqrt{a}} \tag{17}$$

The HDV expected total energy consumption E_2^{HDV} [kWh] can then be computed.

$$E_2^{HDV} = D_2^{LH}z_{LH}^{HDV} + D_2^L z_L^{HDV} \tag{18}$$

T_2^{HDV} [veh-h] is the total time worked by the HDV fleet in this two-echelon delivery scenario.

$$T_2^{HDV} = \frac{D_2^{LH}}{\bar{v}_{LH}^{HDV}} + \frac{D_2^L}{\bar{v}_L^{HDV}} + \delta A\tau_{LU}^{HDV} \tag{19}$$

Finally, the expected HDV fleet size N_2^{HDV} is equal to

$$\begin{cases} If \ \frac{E_2^{HDV}}{BC^{HDV}} \geq \frac{T_2^{HDV}}{H}; N_2^{HDV} = \left[\frac{T_2^{HDV} + \frac{E_2^{HDV}}{P_c^{HDV}}}{H + \frac{BC^{HDV}}{P_c^{HDV}}}\right]^+ \\ \\ If \ \frac{E_2^{HDV}}{BC^{HDV}} \leq \frac{T_2^{HDV}}{H}; N_2^{HDV} = \left[\frac{T_2^{HDV}}{H}\right]^+ \end{cases} \tag{20}$$

Where P_c^{HDV} [kW] is the HDV battery charging power.

The expected number of parcels delivered between two HDV fleet replacements r_2^{HDV} (see Fig. 1) is given in Equation (21) (see the Supplementary Information, section 3, Result 2).

$$r_2^{HDV} = \delta A \bullet min\left\{\frac{CL^{HDV}BC^{HDV}N_2^{HDV}}{E_2^{HDV}}; \frac{L^{HDV}N_2^{HDV}}{D_2^{LH} + D_2^L}\right\} \tag{21}$$

2.2.6. ADR operation modelling

We start by computing the expected distance ρ_h [km] between a micro-hub and the location of the first receiver along an ADR route (see the Supplementary Information, section 3, result 4). We assume that the total demand density δ [receivers/km^2/day] is uniformly distributed all over the service region.

$$\rho_h = \frac{\sqrt{a}}{2} \tag{22}$$

l_2^{ADR} [km] is the expected distance between two consecutive delivery points (Daganzo, 1984).

$$l_2^{ADR} = \frac{k^{ADR}}{\sqrt{\delta}}$$
(23)

Where k^{ADR} is the expected routing factor of an ADR.

We estimate the expected time needed per parcel delivery t_2^{ADR} as

$$t_2^{ADR} = \frac{l_2^{ADR}}{\overline{v}_L^{ADR}} + \tau_d^{ADR}$$
(24)

Where $\overline{v}_L^{ADR}$ [km/h] is the ADR commercial speed (calculation can be found in the Supplementary Information, section 2) and τ_d^{ADR} [h] the expected time needed to deliver a parcel to a final customer during the hand-over process.

The next step is to evaluate the expected number of visited receivers per ADR route Ψ_2^{ADR} [receivers], which is mainly restricted by the limited volume capacity of an ADR C^{ADR} [m^3], the operation time window H [h] and the ADR limited battery capacity BC^{ADR} [kWh].

In Equation (25), Ψ_v^{ADR} [receivers] represents the maximum number of receivers that could be visited per ADR route if only the ADR volume capacity restriction were considered.

$$\Psi_v^{ADR} = \frac{C^{ADR}}{E(u)}$$
(25)

If only the time horizon restriction were considered, Ψ_t^{ADR} receivers could be visited along each individual robot route (see the Supplementary Information, section 3, result 5).

$$\Psi_t^{ADR} = \frac{H - \frac{1}{2}\frac{T_2^{HDV}}{N_2^{HDV}} - \frac{2\rho_h}{\overline{v}_L^{ADR}}}{t_2^{ADR}}$$
(26)

Finally, if only the ADR limited battery capacity restriction were considered, Ψ_b^{ADR} receivers could be visited along each ADR route. Ψ_b^{ADR} is the solution of Equation (27).

$$\Psi_b^{ADR}\left[l_2^{ADR}z_L^{ADR}\left(\Psi_b^{ADR}\right) + P_e^{ADR}t_2^{ADR} + z_d^{ADR}\right] + 2\rho_h\left(z_L^{ADR}\left(\Psi_b^{ADR}\right) + \frac{P_e^{ADR}}{\overline{v}_L^{ADR}}\right) = BC^{ADR}$$
(27)

Where P_e^{ADR} [kW] is the ADR electronics power (mostly sensors and processing units), z_d^{ADR} [kWh/delivery] the expected energy required to hand over the parcel to the receiver (some systems using robotic arms are implemented in some robots) and BC^{ADR} the ADR effective battery capacity (still assuming a 80% rate of discharge). Please refer to the Supplementary Information (section 2) for the calculation of z_L^{ADR}.

Here only considering the ADR's "mechanical" energy consumption (see the Supplementary Information, section 2) is not enough. ADRs are autonomous vehicles that need sensors and processing units to work correctly. This electronics equipment requires energy that is taken from the ADR battery, limiting the robot autonomy.

As a consequence, Ψ_2^{ADR} is equal to

$$\Psi_2^{ADR} = min\left\{\Psi_v^{ADR}; \Psi_t^{ADR}; \Psi_b^{ADR}\right\}$$
(28)

The ADR's fleet expected travelled distance per DZ D_2^{ADR} [veh-km] can be computed as

$$D_2^{ADR} = \frac{\delta a}{\Psi_2^{ADR}}\sqrt{a} + k^{ADR}a\sqrt{\delta}$$
(29)

The ADR's fleet expected working time per DZ T_2^{ADR} is estimated as

$$T_2^{ADR} = \frac{D_2^{ADR}}{\overline{v}_L^{ADR}} + \delta a\tau_d^{ADR}$$
(30)

The ADR's fleet total energy consumption per DZ E_2^{ADR} [kWh] is computed.

$$E_2^{ADR} = D_2^{ADR}z_L^{ADR} + T_2^{ADR}P_e^{ADR} + z_d^{ADR}\delta a$$
(31)

We define n_2^{ADR} as the number of ADRs per DZ.

$$
\begin{cases}
If \; \dfrac{E_2^{ADR}}{BC^{ADR}} \geq \dfrac{T_2^{ADR}}{H - \dfrac{1}{2}\dfrac{T_2^{HDV}}{N_2^{HDV}}}; n_2^{ADR} = \left[\dfrac{T_2^{ADR} + \dfrac{E_2^{ADR}}{P_c^{ADR}}}{H - \dfrac{1}{2}\dfrac{T_2^{HDV}}{N_2^{HDV}} + \dfrac{BC^{ADR}}{P_c^{ADR}}} \right]^{+} \\[4em]
If \; \dfrac{E_2^{ADR}}{BC^{ADR}} \leq \dfrac{T_2^{ADR}}{H - \dfrac{1}{2}\dfrac{T_2^{HDV}}{N_2^{HDV}}}; n_2^{ADR} = \left[\dfrac{T_2^{ADR}}{H - \dfrac{1}{2}\dfrac{T_2^{HDV}}{N_2^{HDV}}} \right]^{+}
\end{cases}
\tag{32}
$$

Where P_c^{ADR} [kW] is the ADR's battery charging power.

Consequently, the total size of the ADR's fleet in the whole service region N_2^{ADR} is equal to

$$
N_2^{ADR} = N_h n_2^{ADR}
\tag{33}
$$

The expected number of parcels delivered between two ADR's fleet replacements r_2^{ADR} (see Fig. 1) is given in Equation (34) (see Supplementary Information, section 3, result 2).

$$
r_2^{ADR} = \delta A \bullet min\left\{ \dfrac{CL^{ADR} BC^{ADR} n_2^{ADR}}{E_2^{ADR}}; \dfrac{L^{ADR} n_2^{ADR}}{D_2^{ADR}} \right\}
\tag{34}
$$

Where CL^{ADR} [cycles] is the ADR's battery cycle life, and L^{ADR} [km] the ADR's expected lifespan.

Finally, the optimal value a^* of the DZ area a that minimizes the two-echelon GWP is given in Equation (35) (see the Supplementary Information, section 3, result 6; Robusté et al., 1990).

$$
a^* = \dfrac{1}{1.5} \dfrac{1}{\delta} \left(\dfrac{C^{ADR}}{E(u)} \right)^2
\tag{35}
$$

This optimized value of the DZ area a^* will be used in the rest of the paper.

2.3. Modelling uncertainty

To deal with the uncertainty present in the modelling stage, a Monte Carlo analysis will be done (Perboli et al., 2018). The first stage of the Monte Carlo approach is to assume some given probability distribution functions (PDFs) for the model input parameters. In our case, the input parameters that present more uncertainty and need to be considered in the Monte Carlo approach are:

- The diesel well-to-wheel GWP (Ecoinvent 3.6 database; Ntziachristos & Samaras, 2019).
- The 2020 electricity production mix (Ecoinvent 3.6 database; electricityMap, 2022a, 2022b)
- The line-haul distance between the carrier's DC and the service region (authors' own data; Bunderverband Paket & Express Logistik, 2017)
- The carrier's demand density (Comisión Nacional de los Mercados y la Competencia, 2020; Bunderverband Paket & Express Logistik, 2017)
- The line-haul and local driving cycles (DieselNet, 2022; NREL, 2022).
- The ADR's production GWP (authors' own data; Ecoinvent 3.6 database)
- The ADR's driving cycle smoothing factor (see Supplementary Information, Section 2; Cox et al., 2018)

Then the last-mile operation key performance indicator (KPI) PDFs are obtained by computing the outputs of the analytical model for a very large number of input parameter random samplings. During a Monte Carlo iteration, a value of each input parameter is obtained, based on its own PDF, previously defined. Considering these input values, the different delivery KPI values, including production and use stage GWP, are obtained using the mathematical formulation presented in the previous subsections, and stored for analysis in the simulation post-processing. Considering a statistically representative number of Monte Carlo iterations, the delivery KPI PDFs can be obtained. A more-in depth analysis can be performed with this methodology because the model output is described with a mean value and a standard deviation, corresponding to the model sensitivity analysis.

The Monte Carlo methodology is highly flexible and enables the modelling of non-linear effects. In addition, it is complementary with the continuous approximation approach. Indeed, given a set of input parameters, the computation of the different delivery KPIs does not require the usage of complex and time-consuming numerical optimization techniques, increasing the number of Monte Carlo iterations, which can be performed within a reasonable time. The combination of the Monte Carlo and continuous approximation techniques is thus highly scalable.

3. Case study

After the modelling process of the production and usage stages of the different vehicles, we propose to study two different use cases: the urban cores of Hamburg (HH) and Barcelona (BCN) metropolitan areas. The urban core is understood as a "densely inhabited city"

within a functional urban area (Dijkstra et al., 2019). We believe that comparing these two service regions with distinct characteristics and located in two different European countries will provide insightful results. In this section, detailed information about the parcel and operation input parameters are described.

3.1. Service region and demand characteristics

We only consider parcels whose mass is less than 2 kg and volume inferior to 0.04 m^3 (40 cm × 30 cm × 30 cm box; Swiss Post, 2022). We assume that these type of parcels represent around 50% of the total number of deliveries in the CEP market (Comisión Nacional de los Mercados y la Competencia, 2020) and that the average volume of these parcels is 0.02 m^3 and expected mass 1 kg.

The operation time window H is assumed to be 8 h, which corresponds to a standard shift in the transport industry (Perboli et al., 2018). For fair comparison, the operation time window H is the same in the BAU and two-echelon delivery schemes.

Fig. 5 presents the main characteristics of the two considered service regions. The locations of the different carriers' DCs are also indicated (authors' own data; Bunderverband Paket & Express Logistik, 2017).

The urban core areas of HH and BCN are respectively 739 and 539 km^2. In Fig. 6, the expected line-haul distance ρ_{DC} is displayed for the two service region use cases. It can be seen that the logistics sprawl in BCN is more relevant since the expected line-haul distance between the carriers' DC and the urban cores is higher and the standard deviation is also higher. The distances between all carriers' DCs and urban cores were computed using QGIS 3.22.4 (QGIS Development Team, 2022). The computation of this line-haul distance does not consider the actual road grid of the service region but follows a L2 metrics. In addition, we consider in this case study that all road gradients are null, including line-haul highways and the local grid. As a first approach, this assumption seems to make sense. Nevertheless, to have finer results in the future, road gradient is an important aspect that should be considered, since vehicles travelling on roads with an important gradient will suffer from an increased energy consumption rate per kilometer, hindering their range, especially for BEVs.

Fig. 6 also presents the expected demand density in the HH and BCN urban cores. We assume that this expected demand density follows a triangular PDF, whose minimum, mode and maximum values depend on the service region (Bunderverband Paket & Express Logistik, 2017; Comisión Nacional de los Mercados y la Competencia, 2020).

Finally, Fig. 7 depicts the 2020 electricity mix in Germany and Spain, as well as the corresponding GWP per kWh of energy carrier (electricityMap, 2022a; electricityMap, 2022b; Ecoinvent 3.6 database). We also propose to study the Stated Policies Scenario (STEPS) and Sustainable Development Scenario (SDS) from the International Energy Agency (IEA, 2021) for the year 2050. The values of the GWP per kWh in the different electricity mix scenarios are compared with the well-to-wheel GWP of diesel production. Considering the data taken from the Ecoinvent 3.6 database (activity "diesel production, low-sulphur, petroleum refinery operation" in "Europe without Switzerland"), the expected well-to-tank GWP of 1 kg of diesel is equal to 0.59 kg CO_2-eq. Assuming that 0.083 kg of diesel generates 1 kWh of energy (diesel density of 0.83 kg/L and net heating value of 10 kWh/L), the well-to-tank GWP of diesel production is equal to 0.049 kg CO_2-eq per kWh. In addition, we estimate that the tank-to-wheel GWP of diesel is 3.169 kg CO_2-eq per kg (Ntziachristos & Samaras, 2019), i.e. the tank-to-wheel GWP of diesel is 0.264 kg CO_2-eq per kWh.

3.2. Vehicle characteristics

Table 3 presents the ICE LCV, e-LCV and e-HDV input parameters that were used in the numerical use cases. The volume capacity of both ICE and electric LCVs is assumed to be 3 m^3 (Renault, 2021) whereas the HDV capacity is 20 m^3 (StreetScooter, 2021). The expected stop time per delivery τ_d^{LCV} is 4 min (Allen et al., 2018; Perboli & Rosano, 2019). Considering the lack of data, we considered that the expected unloading time of a parcel at the micro-hub (in the case of the two-echelon distribution) is 30 s. The powertrain efficiency of the electric LCVs and HDVs is 0.81 (Kirschstein, 2020). The ICE LCV idle and fuel consumption was estimated using data from Kirschstein (2020). The routing factor of both LCVs and HDVs is assumed to be 0.7 (Daganzo, 2005). The wheel/road friction
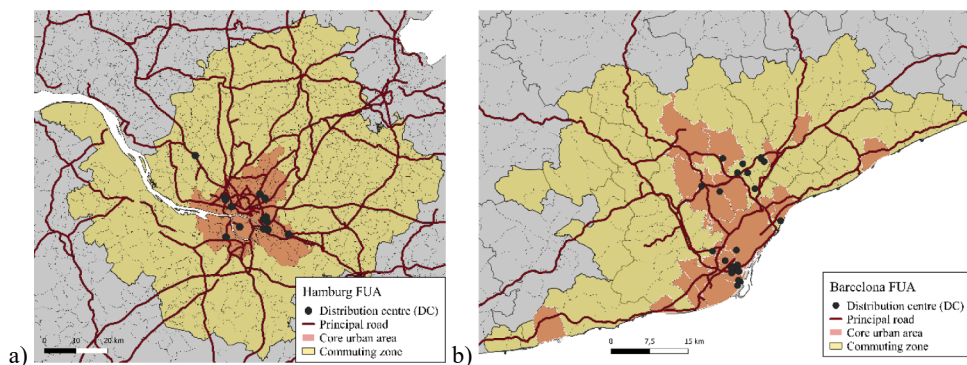

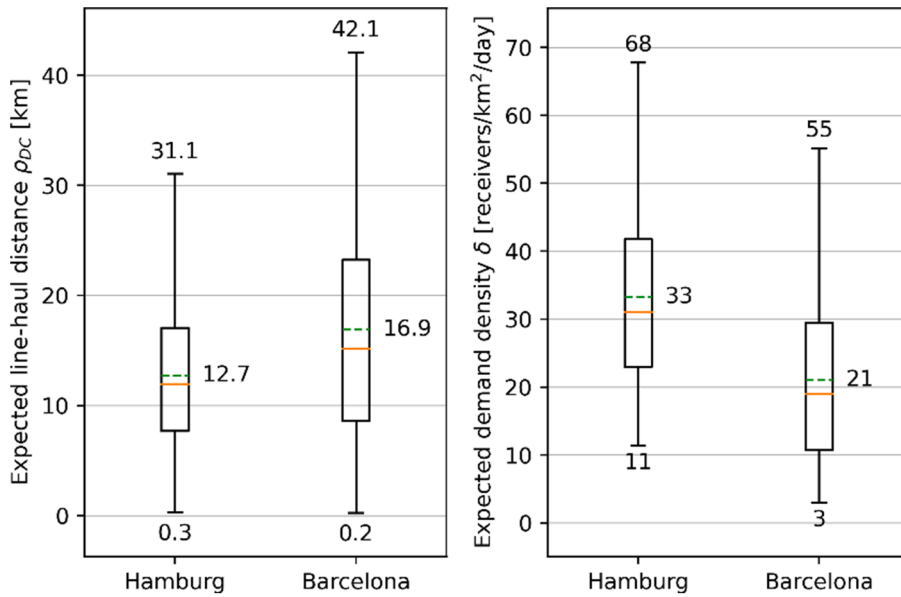
Fig. 5. A. hh and b. bcn service regions.

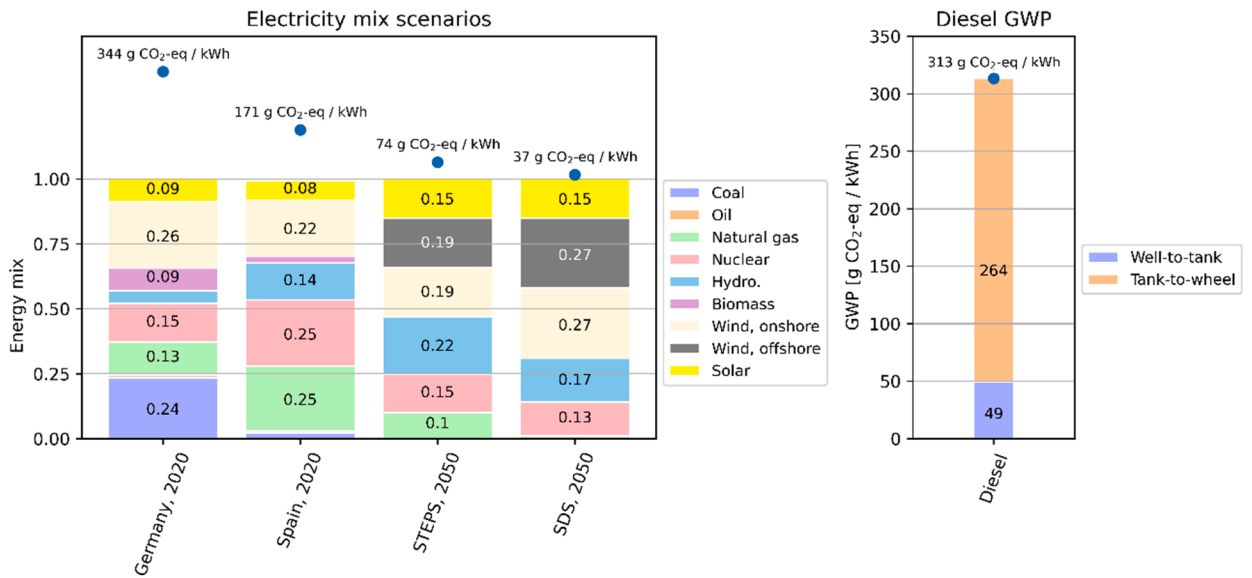**Fig. 6.** Expected line-haul distance and demand density in the HH and BCN urban cores.

Fig. 7. Well-to-wheel GWP of different electricity mix scenarios and diesel.

coefficient c_{roll}^{veh} and aerodynamic drag coefficient C_x^{veh} are taken from Kirschstein (2020). As described in Section 2.2.1 (a) and 2.2.2 (a), the GWP of the different vehicle production (without batteries, in the case of electric vehicles) was calculated using data from Ellingsen et al. (2016), originated from the inventories developed by Hawkins et al. (2012). As for the GWP of battery production, data from the project "BenchBatt", summarized in Melo et al. (2020), was used, considering a LFP battery (the technology from the prototype). Finally, a lifespan of 180,000 km was assumed (Ellingsen et al., 2016).

As for ADRs, we considered six different robots, being ADR 1 our reference for this study (see Table 4). In all defined scenarios, the ADR volume capacity is 0.4 m³ (authors' own data based on the actual robot prototype). The main objective of studying several robot scenarios is to observe how operational conditions can affect the environmental impact of the two-echelon strategy using ADRs. We assumed that all ADRs have the same design but their operations are affected by internal factors (battery technology used to power the robot, sensor technology, or vehicle lifespan) and external ones (expected stop time per delivery or maximum allowed cruising speed). These latter parameters are not directly related to the robot design but they will affect the environmental impact of robot operations.

As previously explained, ADR 1 is our baseline robot. For the remaining robots (ADR 2 to ADR 6), only one input parameter differs

Table 3
LCV and HDV operation input parameters.

Input parameter	ICE LCV	e-LCV	e-HDV
Volume capacity (m^3)	3	3	20
Expected stop time per delivery (min)	4	4	–
Parcel unloading time at micro-hub (min)	–	–	0.5
Powertrain efficiency	–	0.81	0.81
Idle fuel consumption (L/h)	0.51	–	–
Full fuel consumption (L/h)	12.8	–	–
Motor power (kW)	76.8	–	–
Vehicle mass (without battery in case of BEV) (ton)	1.28	1.15	3.41
Wheel/road friction coefficient	0.008	0.008	0.008
Air drag coefficient	0.65	0.65	0.65
Projected front surface (m^2)	3.35	3.35	6
Routing factor	0.7	0.7	0.7
Vehicle lifespan (km)	180.000	180.000	180.000
Battery capacity (kWh)	–	33	76
Battery cycle life (cycles)	–	2.000	2.000
Battery charging power (kW)	–	11	11

Table 4
ADR operation input parameters.

Input parameter	ADR 1	ADR 2	ADR 3	ADR 4	ADR 5	ADR 6
Volume capacity (m^3)	0.4	0.4	0.4	0.4	0.4	0.4
Expected stop time per delivery (min)	3	3	1.5	3	3	3
Powertrain efficiency	0.81	0.81	0.81	0.81	0.81	0.81
Vehicle mass (without battery) (ton)	0.23	0.23	0.23	0.23	0.23	0.23
Wheel/road friction coefficient	0.008	0.008	0.008	0.008	0.008	0.008
Air drag coefficient	0.65	0.65	0.65	0.65	0.65	0.65
Projected front surface (m^2)	1	1	1	1	1	1
Routing factor	0.7	0.7	0.7	0.7	0.7	0.7
Max. allowed speed (km/h)	25	25	25	10	25	25
Vehicle lifespan (km)	40,000	20,000	40,000	40,000	40,000	40,000
Battery mass (ton)	0.025	0.025	0.025	0.025	0.025	0.025
Battery capacity (kWh)	3.0	3.0	3.0	3	3	7.3
Battery cycle life (cycles)	2,000	2,000	2,000	2,000	2,000	714
Battery charging power (kW)	11	11	11	11	11	11
Electronics power (kW)	0.55	0.55	0.55	0.55	0.28	0.55

from ADR 1. This altered parameter is highlighted in Table 4 (see the squares). As a matter of illustration, ADR 2 has exactly the same input parameter as ADR 1 but we assumed that ADR 2 lifespan is twice lower. Our objective is to perform a sensitivity analysis of the models we previously defined.

The ADR battery charging power was overestimated compared to the actual prototype system to simulate fast charging operations. The power needed to supply ADR electronics, used for autonomous navigation, is detailed in Table 5. The energy consumption of ADR "vehicle-to-X" (V2X) communication could also be included under the concept named "electronics power", also integrating 5G technology and data storage in the cloud (Whitehead et al., 2015; Williams et al., 2022). Considering the huge certainty of the telecommunication systems' environmental impact in future years (Williams et al., 2022), we decided to neglect these aspects in this paper. This hypothesis should be refined in future research.

To generate the ADR driving cycle (see the Supplementary Information, section 2), we assume that the robot acceleration rate follows a triangular probability distribution function of minimum value 0.2 m/s^2, mode 0.4 m/s^2 and maximum value 0.7 m/s^2 (Rechkemmer et al, 2019). We assume that the ADR deceleration rate follows a triangular probability distribution function of minimum value 0.3 m/s^2, mode 0.4 m/s^2 and maximum value 0.65 m/s^2 (Rechkemmer et al, 2019). The cruising speed follows a uniform

Table 5
ADR electronics power.

Component	Power	Reference
LiDARs	30 W	Authors' own data
Global Navigation Satellite System (GNSS)	3 W	Authors' own data
Cameras	10 W	Authors' own data
Sonar	Negligible	Authors' own data
Processing units	400 W	Authors' own data; Gawron et al., 2018
Display screens	100 W	Authors' own data
Total	**≈ 550 W**	

probability distribution function between 5 km/h and the ADR allowed maximum speed, which depends on the considered scenario (see Table 4). The ADR prototypes considered in this paper were designed for road, bicycle lane and pedestrian area autonomous navigation. This variety of operative domains is reflected in the ADR's driving cycles (see Supplementary Information, Section 2), especially in the cruising speed of each individual stochastic micro-trip. We consider that the ADR's maximum allowed speed is 25 km/h, except for ADR 4, whose maximum allowed speed is 10 km/h. This maximum allowed speed is not necessarily reached by all individual micro-trips, which are built following a stochastic process. ADR 4 is representative of robot operations restricted to bike lanes and large sidewalks. For all ADR scenarios, the cruising time is assumed to represent 27.5% of the driving cycle total time (Rechkemmer et al, 2019). This rate falls to 12% when considering the idling time (Rechkemmer et al, 2019). The ADR's driving cycle smoothing coefficient α (see Supplemental Information, Equation (1); Cox et al., 2018) is assumed to follow a uniform probability distribution function between 0 and 0.9 (Cox et al., 2018).

Finally, the developed models in this study do not consider the influence of weather conditions on the use stage of the vehicles. As addressed in Egede (2018), the ambient temperature influences the energy consumption of the heating and cooling auxiliaries per kilometer driven, which is of particular relevance when comparing electric with conventional vehicles. In order to understand the impact of geographical and temporal differences on battery's performance, and particularly on the environmental impact of vehicle's operation in HH and BCN regions, the system modelling should couple spatial models with temperature profiles to the LCA foreground system models, following the methodology proposed by Cerdas (2022). Furthermore, snow, rain or fog can affect the behavior of sensors used for autonomous navigation (Zhang et al., 2021), which would hinder the operations of ADRs and prevent them from working correctly. These aspects should be refined in future research.

4. Results

4.1. Cradle-to-grave analysis

Fig. 8 illustrates the contribution analysis of the cradle-to-gate environmental impacts of the production of one ADR. The chassis is the main contributor for GWP (45%), FDP (37%), PMFP (35%), POFP (36%) and TAP (34%). The primary aluminum production mainly drives these impacts, given its high share (88%) in the chassis. In the aluminum production process, electricity production from hard coal and heat generation are the main contributors, due to very energy-intensive stages.

The display equipment also shows relevance across the impact categories, especially in MEP (67%) given by the treatment of wastewater from the liquid crystal display production. Motors and batteries present similar contributions across the impact categories. The highest burdens are present in toxicity-related categories FETP, METP, HTP. The impacts are mostly driven by copper production and the treatment of sulfidic tailings from copper mine operation, which is the mining waste after ore processing to remove the copper. In the case of batteries, their contribution to MDP reaches 23% particularly given the manganese concentrate production.

Even though the other sub-components (e.g. *internal delivery system, electronics, sensors, processing units, shell, brakes, steering, wheels and tires*) show smaller contribution to the analyzed impact categories, their absolute numbers play a role in the total environmental impact of the ADR production. Despite its compacted size and reduced weight, some sub-components are specific to autonomous delivery robots (e.g. *display, electronics, sensors, internal delivery system* etc.), and their total burdens may lead to high impact in comparison with LCVs. Further results can be found in the Supplementary Information (see Table S2).
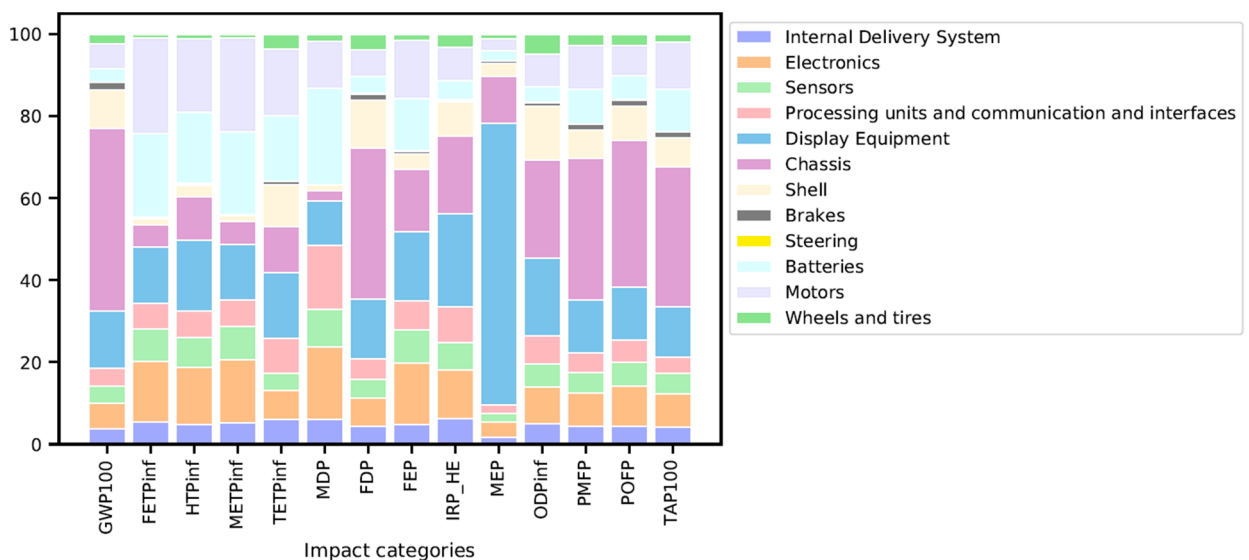

Fig. 8. Environmental impacts' contribution analysis for the production of one ADR. Impact categories are characterized as in the ReCiPe method (see Table 1).

Fig. 9 presents the GWP (in absolute value) of producing one electric HDV, one electric LCV, one ICE LCV or one ADR. The GWP per ton of vehicle is also showed.

Even if the absolute ADR production GWP is twice lower than the e-LCV production GWP (4.5 ton CO_2-eq per ADR against 10.4 ton CO_2-eq per e-LCV), the GWP of producing one ton of ADR is 2.4 times higher than the GWP of producing one ton of e-LCV (17.5 ton CO_2-eq per ton of ADR against 7.3 ton CO_2-eq per ton of e-LCV).

As previously mentioned, this is partly due to the components that are specific to the ADRs. The internal delivery system, electronics, sensors, processing units, communications and interfaces and display equipment represent more than 30% of the ADR production total GWP (see Fig. 8). In addition, the data that was used to model the ADR production concerned a first robot prototype whose design was not necessarily optimized, explaining the higher GWP per ton of vehicle in the case of the ADR.

4.2. Delivery operations key performance indicators

After having derived some insight about the vehicle production, we can present the key performance indicators (KPIs) of the BAU and two-echelon delivery operations in the HH and BCN service regions during the usage stage of the vehicles.

As previously mentioned, some input parameters are stochastic. To deal with this uncertainty, 1,500 simulations were run, following a Monte Carlo approach. As a consequence, we present the different operation KPIs as box plots.

In the BAU delivery scheme, ICE vehicles consume in average 205 Wh of energy per parcel delivery in HH. This figure falls to 98 Wh in the case of e-LCVs, i.e. the energy efficiency of e-LCVs is approximately twice higher as ICE LCVs'. In the case of the BCN service region, ICE LCVs consume, on average, 290 Wh per delivery and e-LCVs 140 Wh per delivery, confirming that e-LCVs are more efficient in the usage stage than ICE LCVs. Delivery vehicles consume more energy per parcel delivery in BCN because the logistics sprawl is bigger and the demand density is lower (see Fig. 6); LCVs have to cover a larger distance to access the service area and also between each recipient.

In the case of the two-echelon distribution scenario, the total energy consumption per parcel delivery is the sum of two terms. On the one hand, electric HDVs have to transport the parcels from the carriers' DCs to the service region. The corresponding energy consumption is equal to, on average, 25 Wh per delivery in HH and 36 Wh per delivery in BCN (see the Supplementary Information, Section 4). On the other hand, we have to consider the energy consumed by the ADRs to take the parcels from the urban micro-hubs to the final receivers. The average ADR's energy consumption ranges from 27 Wh per delivery to 72 Wh per delivery (depending on the ADR's operational conditions) in HH and from 32 Wh per delivery to 91 Wh per delivery in BCN. The higher ADR's energy consumption per parcel delivery in BCN is also due to the lower demand density in this service region.

To sum up, the average total energy consumption (including HDV and ADR) in the two-echelon delivery scheme ranges from 51 Wh per delivery to 97 Wh per delivery in HH and from 68 Wh per delivery to 127 Wh per delivery in BCN (see Fig. 10). Considering our reference ADR 1, the two-echelon delivery scheme is 24% more efficient than the e-LCV BAU scenario in HH in terms of energy consumption in the usage stage. This efficiency improvement reaches 34% in BCN.

If we compare the different ADR's operational conditions, it seems that decreasing the expected stop time per delivery τ_d^{ADR} to 1.5 min would generate a 19% (respectively 15%) decrease of the two-echelon total energy consumption in HH (in BCN, respectively). While idling and waiting for the final recipient, the ADR's sensors consume energy, increasing the expected total energy consumption per parcel delivery. This is confirmed by the ADR 4 and ADR 5 operational scenarios (see the Supplementary Information, section 4). If
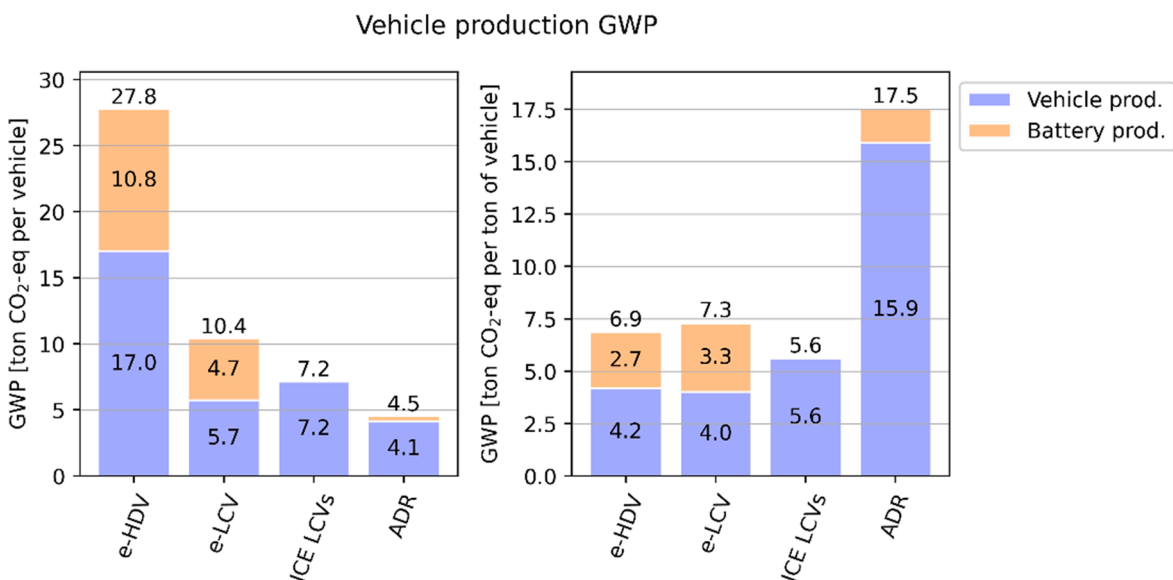

Fig. 9. E-hdv, e-lcv, ice lcvs and adr vehicle production gwp.
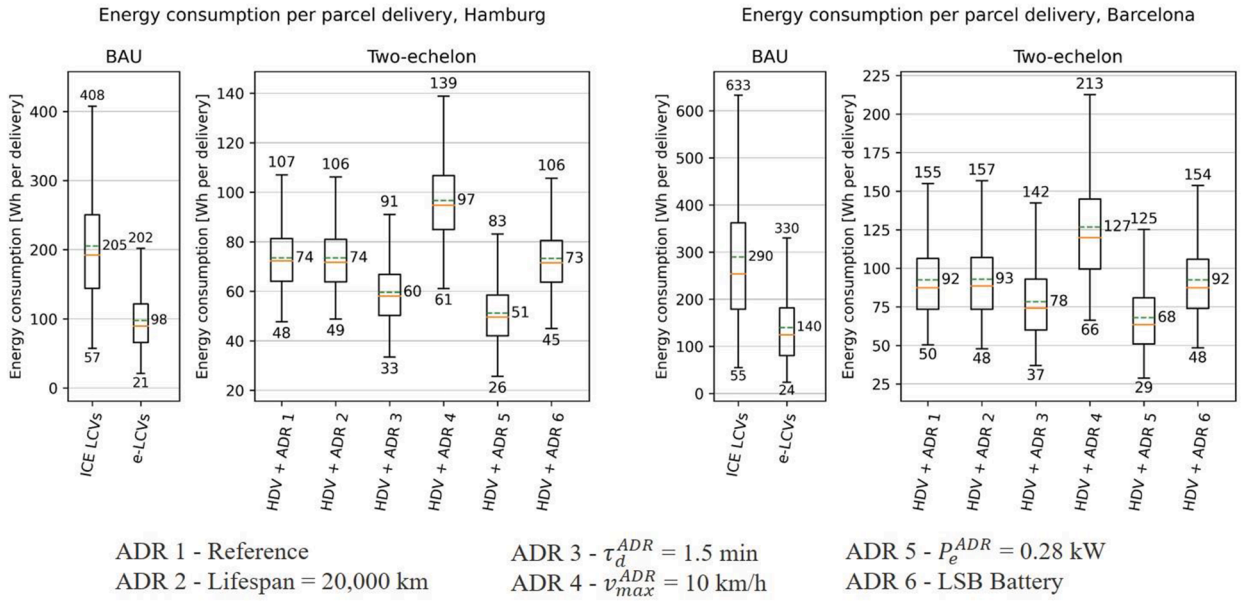
Fig. 10. Energy consumption per parcel delivery during the use stage in the HH and BCN service regions.

the ADR's maximum allowed speed is decreased to 10 km/h (ADR 4), the mechanical energy consumption is lower because the robot goes slower. However, the sensor energy consumption increases because sensors always need to be powered and the delivery time per parcel is increased (because the ADR goes slower). This seems to indicate that sensors represent a higher share of the ADR's energy consumption. In the same line, if the robot sensor power is decreased to 280 W (ADR 5 operational scenario), the ADR's energy consumption per parcel delivery decreases by 45% approximately (see Supplementary Information, Fig. 8), both in HH and in BCN, which confirms the previous statement.

In terms of energy consumption, our results are consistent with Kirschstein (2020). Considering high traffic congestion, 150 customers, a delivery zone radius of 2 km, i.e. a demand density of 12 receivers/km^2, Kirschstein (2020) found that the energy consumption is approximately 300 Wh per delivery in the case of ICE LCVs and around 150 Wh per delivery in the case of e-LCVs, which is consistent with our results. The energy consumption per parcel delivery is lower in HH because of a higher demand density and a lower expected line-haul access distance on metropolitan highways.

Another interesting KPI to be studied is the expected fleet size (see Fig. 11). In the BAU situation, around 240 LCVs are needed on average to serve all customers in HH and around 120 in BCN. The fleet size does not depend on the used powertrain technology, ICE or
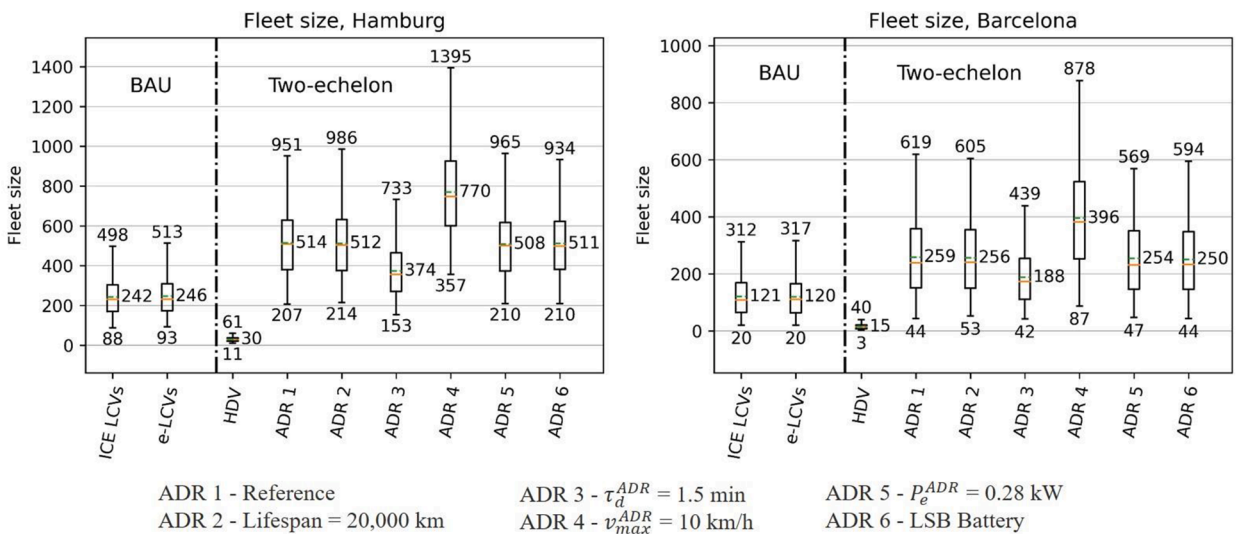

Fig. 11. Expected fleet size in the HH and BCN service regions.

electric engine, because the time constraint is the main factor which defines the LCV fleet size in the BAU delivery scheme (see Equation (12). Battery electric LCVs do not need to be recharged during the day. The fleet size in Barcelona is lower because of the lower demand density to be served in this service region.

In general, 1 LCV in the BAU situation is substituted by 0.1 HDV plus, between 1.5 and 3.3 ADRs, in the two-echelon configuration. In other words, a fleet of 10 LCVs in the BAU delivery scheme can be replaced by 1 HDV plus between 15 and 30 ADRs approximately, depending on the robot operational conditions. To reduce the ADR's fleet size, the ADR stop time per delivery τ_d^{ADR} should be reduced. This result was predictable. If the ADR's maximum allowed speed is reduced to 10 km/h, the ADR's fleet size must be increased in 50% in HH and 53% in BCN, considering that ADR 1 is the reference. The rest of operational parameters have little influence on the ADR's fleet size. The variations that can be observed in Fig. 11 between ADR1, ADR 2, ADR 5 and ADR 6 are essentially due to the Monte Carlo process that generates slight differences in the numerical results.

To understand why so many ADRs are needed to perform the deliveries, we have to consider Equation (32). The number of ADRs operating in a DZ is conditioned by the ADR's operations time window. To be fair with the BAU delivery scheme, we considered that the two-echelon delivery operations had the same time window H. All the HDVs of the two-echelon strategy leave the carrier's DC at time $t = 0$. At time $t = H$, all HDVs must have come back to the DC and all parcels must have been distributed. As a consequence, the HDV time window is H. Nevertheless, the ADR's time window to deliver all parcels in a given DZ is lower than H because before arriving to a given DZ, the HDV has to visit and drop off many parcels in previous DZs. The total time window H has to be split between HDV and ADR operations. In order to decrease the fleet size, the ADR's time window should be increased so that the robots have more time to deliver the parcels. This could be achieved through night deliveries, for instance, because the ADRs would not need any personnel to be operated.

In terms of travelled vehicle-kilometer (see Fig. 12), 1 LCV-kilometer in the BAU delivery operations is substituted by 0.1 HDV-km and 0.7 ADR-km in the two-echelon strategy. In average, implementing logistics micro-hubs would reduce the total travelled distance by 20% approximately, including the distances travelled by both the HDV and ADR fleets in the two-echelon delivery scenario. The travelled distances per parcel delivery are lower in the case of HH because the demand density is higher in the HH service region and the carriers' DCs are located closer to the urban core.

In general, between 100 and 110 receivers are visited by 1 LCV in the BAU delivery scheme. This result is consistent with Allen et al. (2018) and Perboli & Rosano (2019) and means that the time window becomes the most restrictive constraint in the BAU scenario. As a consequence, the expected load factor of a LCV is around 67%, because we assumed the volume capacity of a LCV to be 3 m^3 and the expected volume of a parcel 0.02 m^3. The expected fuel consumptions of ICE LCVs are 0.051 L/km (0.043 kg/km) on metropolitan highways and 0.053 L/km (0.045 kg/km) in the local urban grid (see Supplementary Information, section 2). Considering a diesel net heating value of 10 kWh/L (Kirschstein, 2020), the energy consumption of ICE LCVs is equal to 0.51 kWh/km (line-haul highways) and 0.53 kWh/km (local urban grid). In the case of electric LCVs, the expected energy consumption rates are equal to 0.28 kWh/km on line-haul highways and 0.19 kWh/km in the local urban grid (see Supplementary Information, section 2). These results are consistent with the Electric Vehicle Database (2021). The HDVs unit distance energy consumption rate is equal to 0.65 kWh/km on line-haul metropolitan highways and 0.52 kWh/km in the local urban grid (see Supplementary Information, section 2).

As for ADRs, their load factor is equal to 100% because they are loaded on average with 20 parcels at the logistics micro-hubs. The mechanical propulsion of the robot requires on average around 0.018 kWh/km (see Supplementary Information, section 2) whereas the energy consumption of the electronics equipment is equal to 0.058 kWh/km for our reference case ADR 1 (sensor power of 550 W and commercial cruising speed of 9.5 km/h). Nevertheless, this electronics equipment is also powered while the robot is waiting for the final receiver (while idling the ADR mechanical propulsion energy consumption is null). Considering that an ADR travels around 0.3
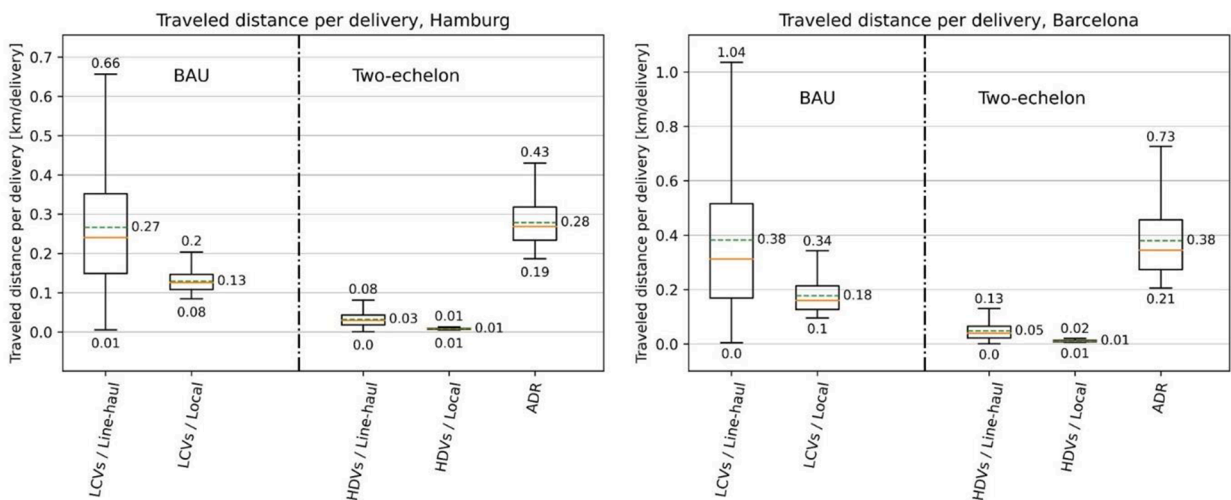

Fig. 12. Expected traveled distances per vehicle type in the HH and BCN service regions.

km per parcel delivery (see Fig. 12), the energy consumption required by the robot's mechanical propulsion is equal to 5 Wh per delivery. For the electronics equipment (considering ADR 1), this value reaches 45 Wh per delivery (including the time needed to travel between two receivers' consecutive locations and the delivery process, considering a stop time of 3 min per delivery). In conclusion, the energy needed to power the ADR's electronics equipment (during the use stage) represents almost 90% of the total energy consumed per parcel delivery, in this model.
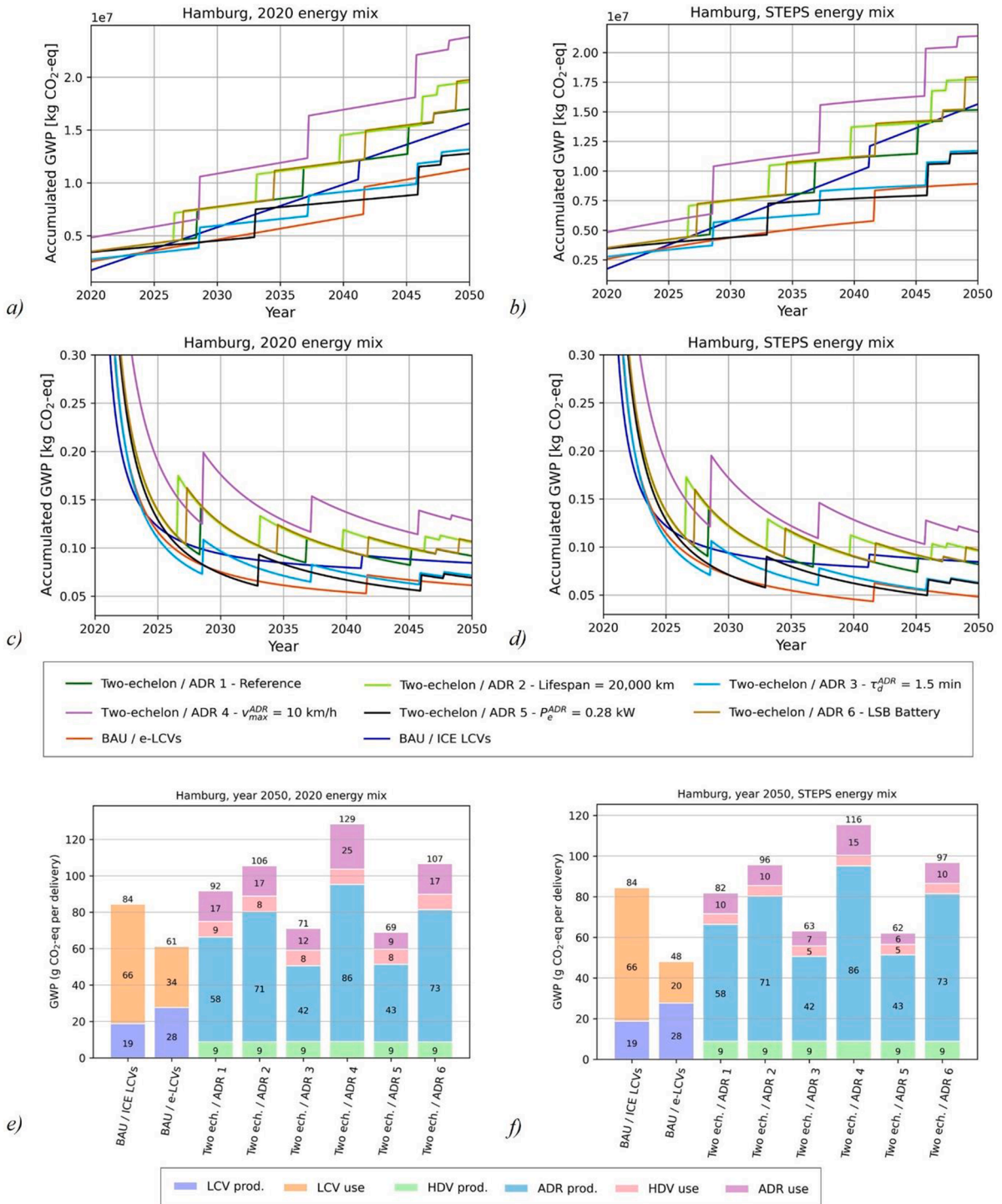

Fig. 13. Life cycle analysis of parcel distribution GWP in the HH service region.
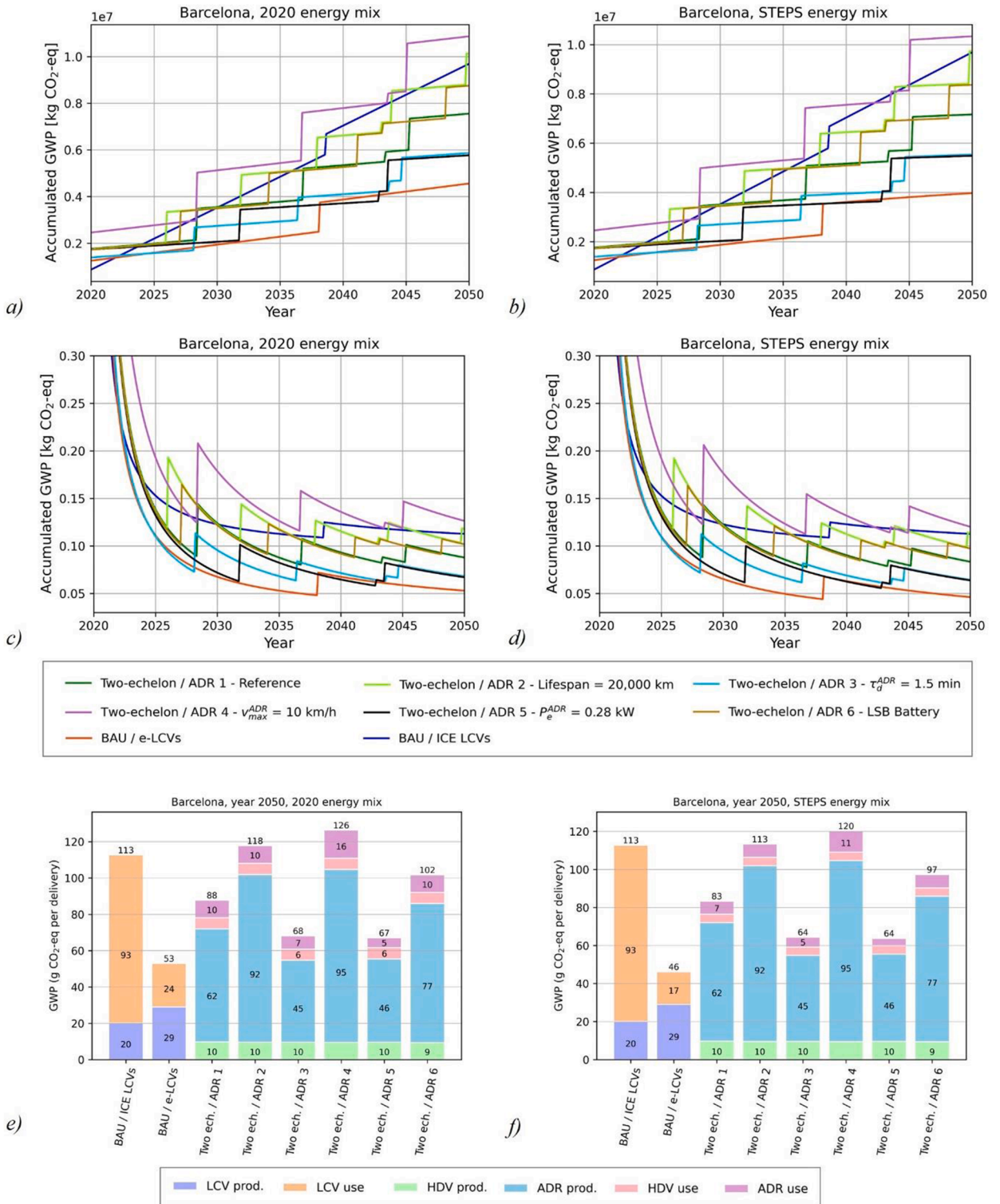
Fig. 14. Life cycle analysis of parcel distribution GWP in the BCN service region.

4.3. Delivery operations LCA

After having analyzed the operational KPIs in the BAU and two-echelon scenarios, it is possible to study the GWP of these two delivery schemes adopting a LCA perspective.

Fig. 13 presents:

- The evolution over time (between 2020 and 2050) of the accumulated GWP of both BAU and two-echelon delivery schemes in the HH service regions in the 2020 and STEP energy mix scenarios (see Fig. 13a and 13b, respectively).
- The evolution over time (between 2020 and 2050) of the unit GWP per parcel delivery of both BAU and two-echelon delivery schemes in the HH service regions in the 2020 and STEP energy mix scenarios (see Fig. 13c and 13d, respectively).
- The unit GWP split between the different vehicle production and use stages at year 2050 in the HH service regions for the 2020 and STEP energy mix scenarios (see Fig. 13e and 13f, respectively).

The discontinuities present in the aforementioned graphs (i.e. Fig. 13a to 13d) correspond to the vehicle fleet replacement. Considering the hypotheses adopted in the modelling stage of the paper, a LCV (either with internal combustion or electric engine) will deliver around 400,000 parcels before its replacement in BCN and around 500,000 in HH (see the Supplementary Information, Fig. 9). In the case of the two-echelon delivery scheme, each individual ADR will deliver between approximately 56,000 and 116,000 parcels before replacement in BCN and between 67,000 and 150,000 parcels in Hamburg, depending on the considered ADR. The main impact factor for the robot fleet replacement is the battery limited number of cycles and capacity (see Equation (34) because all ADRs except ADR 2 have the same mechanical lifespan.

The main results from Fig. 13 are the following. Firstly, moving from ICE LCVs to electric LCVs in the BAU situation would decrease the GWP of parcel distribution in approximately 27% if the German energy mix remains the same between 2020 and 2050 (see Fig. 13e). In the case of the STEPS energy mix scenario, the electrification of the LCV fleet would generate a 43% decrease of the parcel distribution GWP (see Fig. 13f). No significant improvement would be seen in the case of the SDS energy mix scenario (see the Supplementary Information, Fig. 10). During the LCV electrification process, we can observe a shift of the environmental burden from the usage stage to the vehicle production (as illustrated in Fig. 13e and 13f) phase. In BAU deliveries with ICE LCVs, the vehicle production stage represents 23% of the life-cycle total GWP whereas the usage stage accounts for the rest of the GWP, i.e. 77% (see Fig. 13e). If the LCV fleet is electrified, considering that the German electricity mix gradually passes from the current one (in 2020) to the STEPS energy mix (in 2050), the e-LCV production environmental burden would represent 58% of the delivery total GWP whereas the usage stage emissions would represent 42% of the total GWP (see Fig. 13f).

As for the two-echelon delivery scheme using ADRs, the results we obtain are more contrasted. On the period 2020–2050, considering our reference ADR (ADR 1), two-echelon operations would generate around 92 g CO_2-eq per parcel delivery with the 2020 German mix and around 82 g CO_2-eq per parcel delivery in the STEPS energy mix scenario. If the ADR lifespan is lower (ADR 2), the two-echelon operation emissions would be around 100 g CO_2-eq, higher than the BAU delivery scheme with ICE LCVs (see Fig. 13f).

This high environmental impact of the two-echelon operations is due to the very large fleet of ADRs that is needed to perform the operations (see Fig. 11). The environmental burden of ADR 1 production in the STEPS scenario represents 71% of the total two-echelon GWP, followed by the ADR's usage stage GWP (12%), the HDV's production GWP (11%) and the HDV's usage stage GWP (6%).

The two-echelon usage stage GWP is directly related to the usage stage energy consumption that we described in Fig. 10. The ADR's production GWP in the two-echelon delivery scheme depends on the considered operation scenarios. In the case of ADR 2 with a lifespan of 20,000 km, ADR's production have a higher environmental burden because the robot fleet replacement would occur before (see Fig. 13c and 13d). ADR 3′s production environmental burden would be lower than in the ADR 1 scenario because of the ADR 3′s lower fleet size. Two-echelon operations based on ADR 4 would have the highest environmental burden because of ADR 4′s huge fleet. Deliveries with ADR 5 would have the lowest GWP. Even if ADR 5′s fleet size would be similar to ADR 1′s, ADR 5′s fleet replacement occurs afterwards (see Fig. 13c and 13d). If all ADR fleets were first replaced before 2030, ADR 5 would be the only one to have its first replacement between 2030 and 2035 (see Fig. 13c and 13d). In the case of ADR 5, the energy consumption per parcel delivery is lower, i.e. the factor which limits the robot lifetime is the mechanical pieces limited lifespan and not the battery's total number of cycles (see Equation (34), as in other robotic scenarios.

Finally, substituting ADR 1 battery with a LSB one would increase the two-echelon total GWP (see ADR 6 scenario) by 17% approximately. Even if the LSB battery capacity is higher than the LFP one (implemented in ADR 1), its total number of cycles is lower, and ADR 6′s fleet replacement would take place on a reduced time basis (see Fig. 13c and 13d).

For the case of the BCN service region, the results are presented in Fig. 14. A similar insight previously developed in the case of the HH service region is gained.

Using electric LCVs in the BAU scenario contributes to a 53% reduction of the total GWP per delivery if we assume that the 2020 Spanish mix does not evolve over time (see Fig. 14e). The 2020 Spanish energy mix generates around 170 g CO_2-eq per kWh against 344 g CO_2-eq per kWh for the 2020 German electricity mix (see Fig. 7).

In the case of the ADR's two-echelon operations, the conclusions do not vary from the HH's service region insight we previously obtained since the total GWP combining HDVs and ADRs lies between 64 and 126 g CO_2-eq per parcel delivery, which is equivalent to the values we obtained in the case of HH. Even if the Spanish electric mix has a lower GWP, the lower logistics economies of scale in BCN (because of a lower demand density) limits the two-echelon efficiency improvement.

As we previously described, the main two-echelon GWP source is the ADR production (see Fig. 14e and 14f). In this Barcelona use case, the ADR's production GWP represents around 75% of the two-echelon total GWP in the case of ADR 1 and the STEPS energy mix.

This increased share of the production GWP for electric vehicles (both e-LCVs, e-HDVs and ADRs) is due to the lower GHG emission rate per kWh of electricity in Spain, decreasing the weight of the usage stage energy consumption GWP.

4.4. Main managerial insights

The electrification of the LCV fleet following a BAU operational scheme would decrease the parcel delivery GWP by 59% in Barcelona and 43% in Hamburg (considering the STEPS electricity mix scenario). Compared with e-LCV BAU operations, the two-echelon ADR-based operational scheme is not competitive in terms of parcel delivery GWP. In both the Hamburg and Barcelona service regions, the two-echelon delivery strategy with our reference ADR would generate between 80 and 90 g CO_2-eq per parcel delivery. This high figure is essentially due to the ADR's production high environmental burden. Individually, the production of each ADR generates a significant amount of GHG because of some components that are inherent to autonomous technologies. In addition, the ADR fleet needed to serve all the demand in a restrictive time window is huge. The higher production GWP associated with a bigger fleet explains why the environmental burden of the ADR's production is so high in the delivery process. During the use stage, the two-echelon ADR-based delivery method is undoubtedly more efficient because the energy consumption per parcel delivery in the use stage is decreased by more than 25% in the two-echelon model when compared with the e-LCV BAU delivery method.

As a consequence, the main leverages to decrease the GWP of a two-echelon delivery scheme combining HDVs and ADRs are:

- The improvement of the ADR's production processes to limit GHG emissions during the robot production phase.
- The reduction of the ADR's electronics and sensor power. This measure could reduce both the ADR's production and usage stage GWP. In the usage stage, a reduction of the ADR's electronics and sensor power would limit the total energy consumption of the two-echelon delivery scheme. As for the ADR's production environmental burden, a reduction of the electronics and sensor power increases the ADR's lifetime and the robot fleet does not need to be replaced so often. By reducing the sensor and electronics power, the number of battery recharging processes are reduced and the ADR's battery lifetime can be maximized since the robot battery lifetime is the factor which conditions the robot fleet replacement in our model. This improvement could also be achieved through the increase of the ADR's battery capacity, limiting the number of recharging cycles, and maximizing the battery lifetime.
- The improvement and optimization of the ADR's logistics models. In the formulation we proposed, the main factor explaining the low performance of ADR-based two-echelon delivery schemes is the high ADR's fleet size. To make ADRs more competitive, the fleet size should be reduced. This reduction might be achieved through the optimization of the ADR's logistics operations (as can be the reduction of the stop time per delivery which depends on the delivery process to recipient, as a matter of illustration) and a higher ADR's delivery time window. To widen the ADR's delivery time window, it seems that the decoupling between HDV operations linking all logistics micro-hubs (which could be done at night for instance) and ADR operations (during daytime) would be the most efficient strategy.

5. Conclusion and further research

A life-cycle analysis (LCA) of different distribution strategies within the e-commerce market has been proposed in this paper. A two-echelon delivery pattern combining heavy-duty vehicles (HDVs) and autonomous delivery robots (ADRs) has been compared to business-as-usual (BAU) operations with internal combustion engine (ICE) or electric light commercial vehicles (LCVs). To model the ADR's production, primary data from an actual ADR prototype combined with the ecoinvent database has been used. The mathematical formulation of the usage stage main key performance indicators (KPIs) has been done using the continuous approximation (CA) technique. Finally, combining the production and usage stage modelling, managerial insight, concerning parcel distribution in the Barcelona and Hamburg urban cores, has been obtained. The analysis also shows the impact of the delivery use case in the last-mile operations global warming potential (GWP). The introduction of ADRs on a large-scale basis may not reduce the GWP of last-mile parcel delivery, if a series of operative conditions are not met.

As further research, some underlying assumptions need to be further investigated to make our study more exhaustive. As it was previously mentioned, the ADR's production represents the main part of the two-echelon delivery GWP. In our modelling, we consider that the ADR's production GWP remains constant between 2020 and 2050 and equal to its value in 2020. Considering all the investments that are done in renewable energies, this assumption seems too strong since the energy mix will become greener over the years and this reduction of the well-to-wheel electricity mix GWP should also be considered into the ADR's production since electricity is used to produce a robot. In this case, this evolution could play in favor of ADRs since the robot fleet is replaced more often. A LCV is replaced every 20 years more or less, so its production process cannot benefit from the electricity mix GWP reduction over the years.

In addition, the energy consumption model of the vehicles considered in this study should be improved to take into account the road slope or the environment temperature that can have an influence on the energy consumption per km, especially in the case of battery electric vehicles. Still in the usage stage formulation, CA models should be further refined because the demand densities we dealt with in the paper are at the limit of the CA methodology representative domain.

The two previously mentioned improvements concern the usage stage modelling. It seems reasonable to assume that these improvements would not fundamentally modify the obtained results because of the high ADR's production environmental burden, on which robot manufacturers should be focusing. Concerning the robot production modelling, it has to be mentioned that the data we used was taken from an ADR prototype whose design was not optimized. It can be assumed that in the further iterations of the ADR's design process, further weight improvements will be done, i.e. reducing its production GWP.

Finally, in the fleet replacement modelling, vehicle lifespan would also depend on time, not only distances, as we have been

assuming. It would especially be the case for the ADR's sensors whose lifespan is measured in terms of working hours, not kilometers. In addition, many cities implement vehicle access restrictions such as low-emission zones that depend on the vehicle age. It is being progressively forbidden for old internal combustion engine vehicles to enter city centers. Concerning future research, urban last-mile parcel delivery using drones should also be subject of investigation, analyzing a hybrid delivery solution, potentially combining them with ADRs.

Declaration of Competing Interest

The authors declare that they have no known competing financial interests or personal relationships that could have appeared to influence the work reported in this paper.

Acknowledgements

Appendix A. Supplementary material

Supplementary data to this article can be found online at https://doi.org/10.1016/j.trd.2023.103842.

References

Allen, J., Piecyk, M., Piotrowska, M., McLeod, F., Cherrett, T., Ghali, K., Austwick, M., 2018. Understanding the impact of e-commerce on last-mile light goods vehicle activity in urban areas: The case of London. Transp. Res. Part D: Transp. Environ. 61, 325–338.

Alyassi, R., Khonji, M., Karapetyan, A., Chau, S.C.K., Elbassioni, K., Tseng, C.M., 2022. Autonomous recharging and flight mission planning for battery-operated autonomous drones. IEEE Trans. Autom. Sci. Eng. 20 (2), 1034–1046.

Baldacci, R., Mingozzi, A., Roberti, R., 2012. Recent exact algorithms for solving the vehicle routing problem under capacity and time window constraints. Eur. J. Oper. Res. 218 (1), 1–6.

Bruni, M.E., Khodaparasti, S., Perboli, G., 2023. Energy Efficient UAV-Based Last-Mile Delivery: A Tactical-Operational Model With Shared Depots and Non-Linear Energy Consumption. IEEE Access 11, 18560–18570.

Bunderverband Paket & Express Logistik, 2017. Innovationen auf der letzen meile. Accessed 2021–06-29. Retrieved from https://www.biek.de/presse/meldung/kep-branche-setzt-auf-innovationen-f%C3%BCr-eine-nachhaltige-stadtlogistik.html.

Cerdas, F., 2022. Integrated Computational Life Cycle Engineering for Traction Batteries. Springer International Publishing.

Cerdas, F., Juraschek, M., Thiede, S., Herrmann, C., 2017. Life cycle assessment of 3D printed products in a distributed manufacturing system. J. Ind. Ecol. 21 (S1), S80–S93.

Cerdas, F., Titscher, P., Bognar, N., Schmuch, R., Winter, M., Kwade, A., Herrmann, C., 2018. Exploring the effect of increased energy density on the environmental impacts of traction batteries: A comparison of energy optimized lithium-ion and lithium-sulfur batteries for mobility applications. Energies 11 (1), 150.

Cobert, A., 2009. Environmental comparison of Michelin Tweel and pneumatic tire using life cycle analysis. Georgia Institute of Technology). Doctoral dissertation.

Comisión Nacional de los Mercados y la Competencia (2020). Análisis del sector postal y del sector de mensajería y paquetería 2019. Retrieved from https://www.cnmc.es/expedientes/infdtsp03820.

Cox, B., Mutel, C.L., Bauer, C., Mendoza Beltran, A., van Vuuren, D.P., 2018. Uncertain environmental footprint of current and future battery electric vehicles. Environ. Sci. Tech. 52 (8), 4989–4995.

Cucinotta, F., Guglielmino, E., Sfravara, F., 2017. Life cycle assessment in yacht industry: A case study of comparison between hand lay-up and vacuum infusion. J. Clean. Prod. 142, 3822–3833.

Daganzo, C.F., 1984. The length of tours in zones of different shapes. Transp. Res. B Methodol. 18 (2), 135–145.

Daganzo, C., 2005. Logistics systems analysis. Springer Science & Business Media.

Daganzo, C.F., Gayah, V.V., Gonzales, E.J., 2012. The potential of parsimonious models for understanding large scale transportation systems and answering big picture questions. EURO Journal on Transportation and Logistics 1 (1–2), 47–65.

DieselNet (2022). Emission Test Cycles. Accessed 2022-05-25. Retrieved from https://dieselnet.com/standards/cycles/index.php.

Dijkstra, L., H. Poelman and P. Veneri (2019), "The EU-OECD definition of a functional urban area", OECD Regional Development Working Papers, No. 2019/11, OECD Publishing, Paris.

Egede, P., 2018. Environmental assessment of lightweight electric vehicles. Springer International Publishing.

Electric Vehicle Database, 2021. Electric Vehicle Database. Accessed 2021–12-28. Retrieved from https://ev-database.org/#sort:path~type~order=. rank~number~desc|bodyshape-checkbox-dropdown:pathGroup=.shape-spv|range-slider-range:prev~next=0~1200|range-slider-acceleration: prev~next=2~23|range-slider-topspeed:prev~next=110~450|range-slider-battery:prev~next=10~200|range-slider-eff:prev~next=100~300|range-slider-fastcharge:prev~next=0~1500|paging:currentPage=0|paging:number=9.

electricityMap (2022a). 2020 Spanish energy mix data [Data file]. Accessed 2022-05-25.

electricityMap (2022b). 2020 German energy mix data [Data file]. Accessed 2022-05-25.

Ellingsen, L.A.W., Singh, B., Strømman, A.H., 2016. The size and range effect: lifecycle greenhouse gas emissions of electric vehicles. Environ. Res. Lett. 11 (5), 054010.

Figliozzi, M.A., 2020. Carbon emissions reductions in last mile and grocery deliveries utilizing air and ground autonomous vehicles. Transp. Res. Part D: Transp. Environ. 85, 102443.

Gawron, J.H., Keoleian, G.A., De Kleine, R.D., Wallington, T.J., Kim, H.C., 2018. Life cycle assessment of connected and automated vehicles: sensing and computing subsystem and vehicle level effects. Environ. Sci. Tech. 52 (5), 3249–3256.

Goedkoop, M., Heijungs, R., Huijbregts, M., Schryver, A., Struijs, J., Zelm, R., 2013. ReCiPe 2008: A life cycle impact assessment method which comprises harmonised category indicators at the midpoint and the endpoint level. First edition.

Hauschild, M.Z., Rosenbaum, R.K., Olsen, S.I., 2018. Life Cycle Assessment. Springer International Publishing, Cham.

Hawkins, T.R., Singh, B., Majeau-Bettez, G., Strømman, A.H., 2013. Comparative environmental life cycle assessment of conventional and electric vehicles. J. Ind. Ecol. 17 (1), 53–64.

Hollingsworth, J., Copeland, B., Johnson, J.X., 2019. Are e-scooters polluters? The environmental impacts of shared dockless electric scooters. Environ. Res. Lett. 14 (8), 084031.

Iea, 2021. World Energy Outlook 2021, IEA, Paris. Retrieved from. https://www.iea.org/reports/world-energy-outlook-2021.

Kemp, N.J., Keoleian, G.A., He, X., Kasliwal, A., 2020. Life cycle greenhouse gas impacts of a connected and automated SUV and van. Transp. Res. Part D: Transp. Environ. 83, 102375.

Kirschstein, T., 2020. Comparison of energy demands of drone-based and ground-based parcel delivery services. Transp. Res. Part D: Transp. Environ. 78, 102209.

Koiwanit, J., 2018. Analysis of environmental impacts of drone delivery on an online shopping system. Adv. Clim. Chang. Res. 9 (3), 201–207.

Li, L. He, X., Keoleian, G.A., Kim, H. C., Kleine, R.; Wallington, T. J., Kemp, N. J. (2021). Life Cycle Greenhouse Gas Emissions for Last-Mile Parcel Delivery by Automated Vehicles and Robots. *Environmental science & technology*.

Liu, Y., 2023. Routing battery-constrained delivery drones in a depot network: A business model and its optimization–simulation assessment. Transportation Research Part C: Emerging Technologies 152, 104147.

Marmiroli, B., Venditti, M., Dotelli, G., Spessa, E., 2020. The transport of goods in the urban environment: A comparative life cycle assessment of electric, compressed natural gas and diesel light-duty vehicles. Appl. Energy 260, 114236.

Melo, S.P., Cerdas, F., Barke, A., Thies, C., Spengler, T.S., Herrmann, C., 2020. Life Cycle Engineering of future aircraft systems: the case of eVTOL vehicles. Procedia CIRP 90, 297–302.

Melo, S.P., Cerdas, F., Barke, A., Thies, C., Spengler, T.S., Herrmann, C., 2022. Life Cycle Engineering Modelling Framework for batteries powering electric aircrafts–the contribution of eVTOLs towards a more sustainable urban mobility. Procedia CIRP 105, 368–373.

Nrel, 2022. DriveCAT: Drive Cycle Analysis Tool. Accessed 2022–05-25. Retrieved from. https://www.nrel.gov/transportation/drive-cycle-tool/.

Ntziachristos, L., & Samaras, Z. (2019). EMEP/EEA air pollutant emission inventory guidebook 2019, 53 (9).

Pani, A., Mishra, S., Golias, M., Figliozzi, M., 2020. Evaluating public acceptance of autonomous delivery robots during COVID-19 pandemic. Transp. Res. Part D: Transp. Environ. 89, 102600.

Park, J., Kim, S., Suh, K., 2018. A Comparative Analysis of the Environmental Benefits of Drone-Based Delivery Services in Urban and Rural Areas. Sustainability 10 (3), 888.

Perboli, G., Rosano, M., Saint-Guillain, M., Rizzo, P., 2018. Simulation–optimisation framework for City Logistics: an application on multimodal last-mile delivery. IET Intel. Transport Syst. 12 (4), 262–269.

Perboli, G., Rosano, M., 2019. Parcel delivery in urban areas: Opportunities and threats for the mix of traditional and green business models. Transportation Research Part C: Emerging Technologies 99, 19–36.

Swiss Post (2022). Factsheet. Starship Delivery Robot. Accessed 2022-05-18. Retrieved from https://www.post.ch/-/media/post/ueber-uns/medienmitteilungen/ 2017/factsheet-lieferroboter.pdf?la=en.

QGIS Development Team (2022). QGIS Geographic Information System. Open Source Geospatial Foundation Project. https://www.qgis.org/en/site/index.html.

Rechkemmer, S.K., Zang, X., Zhang, W., Sawodny, O., 2019. In: Towards a Shanghai Electric Two-wheeler Cycle (SE2WC). IEEE, pp. 319–324.

Renault (2021). Renault kangoo e-tech eléctrico. Accessed 2021-11-22. Retrieved from https://empresas.renault.es/electricos/kangoo-electrico.html.

Robusté, F., Daganzo, C.F., Souleyrette II, R.R., 1990. Implementing vehicle routing models. Transp. Res. B Methodol. 24 (4), 263–286.

Soysal, M., Bloemhof-Ruwaard, J.M., Bektaş, T., 2015. The time-dependent two-echelon capacitated vehicle routing problem with environmental considerations. Int. J. Prod. Econ. 164, 366–378.

Stolaroff, J.K., Samaras, C., O'Neill, E.R., Lubers, A., Mitchell, A.S., Ceperley, D., 2018. Energy use and life cycle greenhouse gas emissions of drones for commercial package delivery. Nat. Commun. 9 (1), 409.

StreetScooter (2021). StreetScooter WORK XL. Accessed 2021-11-22. Retrieved from https://www.streetscooter.com/wp-content/uploads/2018/09/sco12308_flyer_ iaa_work_xl_rz_web.pdf.

Torabbeigi, M., Lim, G.J., Kim, S.J., 2020. Drone delivery scheduling optimization considering payload-induced battery consumption rates. J. Intell. Rob. Syst. 97, 471–487.

Whitehead, B., Andrews, D., Shah, A., 2015. The life cycle assessment of a UK data centre. Int. J. Life Cycle Assess. 20 (3), 332–349.

Williams, L., Sovacool, B.K., Foxon, T.J., 2022. The energy use implications of 5G: Reviewing whole network operational energy, embodied energy, and indirect effects. Renew. Sustain. Energy Rev. 157, 112033.

Yowtak, K., Imiola, J., Andrews, M., Cardillo, K., Skerlos, S., 2020. Comparative life cycle assessment of unmanned aerial vehicles, internal combustion engine vehicles and battery electric vehicles for grocery delivery. Procedia CIRP 90, 244–250.

Zhang, Y., Carballo, A., Yang, H., Takeda, K., 2021. Autonomous driving in adverse weather conditions: A survey. arXiv preprint arXiv:2112.08936.